12-2021

Developing a Prototype Energy Harvesting Device for Powering Wireless Onboard Condition Monitoring Sensor Modules for Railway Service

Martin Amaro Jr.
The University of Texas Rio Grande Valley

Recommended Citation

Amaro, Martin Jr., "Developing a Prototype Energy Harvesting Device for Powering Wireless Onboard Condition Monitoring Sensor Modules for Railway Service" (2021). *Theses and Dissertations*. 817.
https://scholarworks.utrgv.edu/etd/817

DEVELOPING A PROTOTYPE ENERGY HARVESTING DEVICE FOR POWERING WIRELESS ONBOARD CONDITION MONITORING SENSOR MODULES FOR RAILWAY SERVICE

A Thesis

by

MARTIN AMARO JR.

Submitted in Partial Fulfillment of the

Requirements for the Degree of

MASTER OF SCIENCE IN ENGINEERING

Major Subject: Mechanical Engineering

The University of Texas Rio Grande Valley

December 2021

DEVELOPING A PROTOTYPE ENERGY HARVESTING DEVICE FOR POWERING WIRELESS ONBOARD CONDITION MONITORING SENSOR MODULES FOR RAILWAY SERVICE

A Thesis
by
MARTIN AMARO JR.

COMMITTEE MEMBERS

Dr. Constantine Tarawneh
Chair of Committee

Dr. Heinrich Foltz
Co-Chair of Committee

Dr. Arturo Fuentes
Committee Member

December 2021

ABSTRACT

Amaro Jr., Martin, Developing a Prototype Energy Harvesting Device for Powering Wireless Onboard Condition Monitoring Sensor Modules for Railway Service. Master of Science in Engineering (MSE), December, 2021, 80 pp., 32 tables, 39 figures, 19 references.

An energy harvesting system is being developed to power a wireless bearing health monitoring device. In contrast to other monitoring systems, this wireless monitoring device is a low-powered onboard solution. Powered by a 3.7-Volt lithium-ion battery, the device can continuously function for several months on a single charge. By implementing an energy harvesting system, the life of the battery can be increased reducing the overall maintenance, electronic waste, and time needed to replace the batteries. The harvesting system uses thermoelectric generators to convert the heat generated in the bearings into electricity. The system is composed of aluminum heat sinks, a switching boost converter, and a battery management chip. The harvesting system's performance was validated using dynamic bearing test rigs which closely replicate the conditions seen on the field. A set of test plans were devised using common freight routes to replicate the amount of heat generated in the bearings throughout different speeds and railcar loads. In optimal conditions, the thermoelectric generators can produce upwards of 60 mW before losses, providing enough energy to properly operate most low-powered electronic devices.

DEDICATION

This thesis is dedicated to my loving family for all their endless support. Para mi madre, Andrea, y mi padre, Martin, por enseñarme desde joven la importancia del trabajo duro y la educación. To my sisters, Daisy and Sandra, for setting an example in perusing a higher education and never letting me give up. I would not be the person I am today without any of you.

ACKNOWLEDGMENTS

To my director and research advisor Dr. Constantine Tarawneh. I am truly grateful for the opportunity you have given me in your research center. You have been one of the best educators I have had the pleasure to meet and your commitment to students’ success is second to none. Thank you for all these years of helping me grow as an engineer and as a person.

I want to thank Dr. Heinrich Foltz for his continuous support. I appreciate the time and patience you took working on this project; my success would not be possible without you. I would also like to thank Dr. Arturo Fuentes for your continuous support throughout my academic career. I have learned a lot in your classes and hope to use that knowledge effectively in the industry.

To everyone at the UTCRS, thank you. You have all made my time at the center the best years at this institution. It has been a privilege to have worked with such talented individuals and I wish you all the best in your future careers.

TABLE OF CONTENTS

Page

LIST OF TABLES

LIST OF FIGURES

Page

CHAPTER I

INTRODUCTION AND LITERATURE REVIEW

1.1 Railroad Industry Impact

In North America, and various parts of the globe, rail transportation is still regarded as the best option to deliver large quantities of goods and supplies in an efficient and economic manner. The U.S freight rail network is made of approximately 630 freight railroads that span across 140,000 miles. Seven of the railroads are classified as "Class 1" which operate across multiple states and account for roughly 68% of freight mileage and 94% of railroad revenue [1]. Rail transportation carries a wide range of cargo including gasoline, natural gas, food products, electronics, machinery, pharmaceuticals, vehicles, etc. [2]. In 2017 alone the United States freight transportation industry supported approximately 1.1 million jobs producing $219 billion in economic output, $71 billion in wages, and $26 billion in tax revenue [3]. With the increasing economic activity in the United States, freight shipments are expected to increase from 18.6 billion tons in 2018 to 24.1 billion tons in 2040 [1]. In addition to economic activity, rail transportation provides lower maintenance costs, greenhouse emissions, and energy consumption when compared to highway-based transportation [3].

1.2 Current Wayside Detectors

Railcars travel for millions of miles introducing large amounts of heat and stress to their components for an extended period of time. Railcar bearings are most susceptible to failure as they support the entire weight of the railcar and cargo. From 2010 to 2020, the Federal Railroad

Administration (FRA) reported 65% of axle/bearing related accidents were caused by overheating/defective bearings [4]. Although there are bearing health monitoring systems in place to mitigate such failures, they are reactive in nature and only send out alerts when bearings are nearing failure. The two widely used bearing health monitoring systems that are currently utilized are: The Trackside Acoustic Detection System (TADS^{TM}) and the Hot-Box Detector (HBD).

Figure 1. TADS system on the side of the railroad track [5]

The TADS^{TM} uses an array of microphones set up along both sides of the rail tracks at specific locations to assess bearing defects under nominal operating speeds [6]. Although this system is proficient in detecting bearings with spalls (defect) on their outer ring raceways, it is not as efficient in detecting bearings with spalls on their inner ring raceways, and there are only 18 TADS^{TM} sites in the U.S and Canada [7], which means the many bearings can go their entire service life without passing through one of these sites.

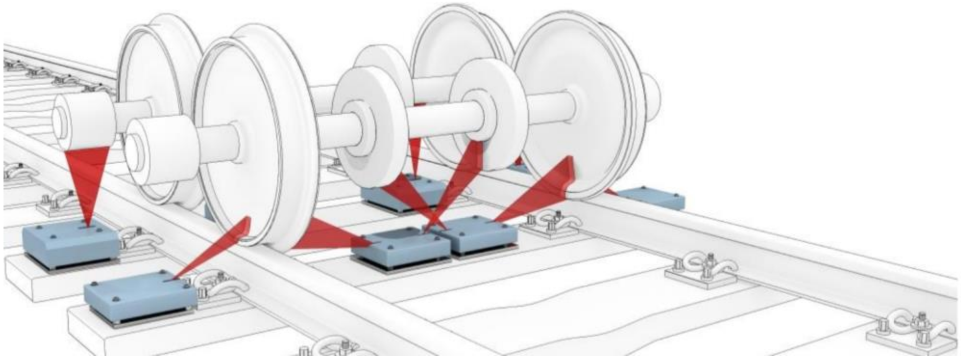

Figure 2. Hot-Box- Detector (HBD) site example [8]

The wayside HBD use non-contact Infrared (IR) sensors to obtain the temperatures of the bearings, axle, and breaks in order to gauge component health. For example, an alarm is triggered if the temperature difference between the bearing surface and the ambient reaches a predetermined threshold set by the Association of American Railroads (AAR). Although HBDs are more prevalent than other forms of bearing condition monitoring systems, with over 6,000 units installed throughout the United States, they have their own sets of drawbacks. HBDs have exhibited inconsistent results by under-or over- predicting bearing operating temperatures. This has led to HBDs flagging false positives and in worst-case scenarios, miss defective bearings that eventually failed catastrophically causing costly train derailments [9].

1.3 Wireless Bearing Condition Monitoring System

Bearing health monitoring technologies are generally categorized as reactive or predictive systems. Reactive systems detect defects as they propagate, raising an alarm to prevent additional damage. In contrast, predictive systems can analyze the condition of the equipment and predict any impendent failure. The team at the University Transportation Center for Railway safety (UTCRS) has developed a prototype wireless onboard condition monitoring module that can continuously gauge bearing health and identify defective bearings at early stages of defect propagation [10]. This prototype design will be installed on each bearing adapter as opposed to existing systems, which sit on the side of the track. The wireless monitoring device is composed of an accelerometer, temperature sensor, and other low power circuitry that will allow the device to operate up to 2 years using a 3.7-volt lithium-ion battery. Due to the nature of the design, the wireless monitoring device requires a consistent and manageable power source to ensure its continuous functionality. This can be accomplished by implementing a suitable energy harvesting device.

1.4 Energy Harvesting Methods

Energy harvesting is based on the principle that there are power losses in all electrical and mechanical systems that can be repurposed or harvested to power other devices. Examples of this include the use of ambient energy from radio transmissions or the vibrations caused by a traveling vehicle to provide a power source by means of power-transforming transducers. To maximize the efficiency of collecting ambient energy, it is important to use a harvesting method that does not completely depend on the varying weather conditions railcars endure. For this specific engineering application, the wasted ambient energy can be seen in two main forms which include the thermal heat generated in railcar bearings and the mechanical vibrations experienced during field service operation. Selecting the most efficient harvesting method will maximize the energy harvested from the system so the power obtained can “trickle” into an intermediate power storage device such as a battery. Electromagnetic vibration, piezoelectric materials, photovoltaic cells, and thermoelectricity have been studied to determine the most viable option for this particular application.

1.4.1 Electromagnetic Vibration Energy Harvesting

The UTCRS first conducted research in energy harvesting applications using magneto-strictive elements and the Villari effect [11]-[12]. A load sensor device developed by Estrada

[11] was able to harvest up to 80 mW of energy under simple harmonic conditions in a laboratory setting. The device contained an alloy, Terfenol-D, that has magneto-strictive properties that cause the material to change shape when exposed to an electromagnetic field. The initial harvesting device was composed of an aluminum spool wound up with 26 AWG wire, an aluminum washer, a Terfenol-D rod, and a 1018 steel notched ring and base as seen in Figure 3.

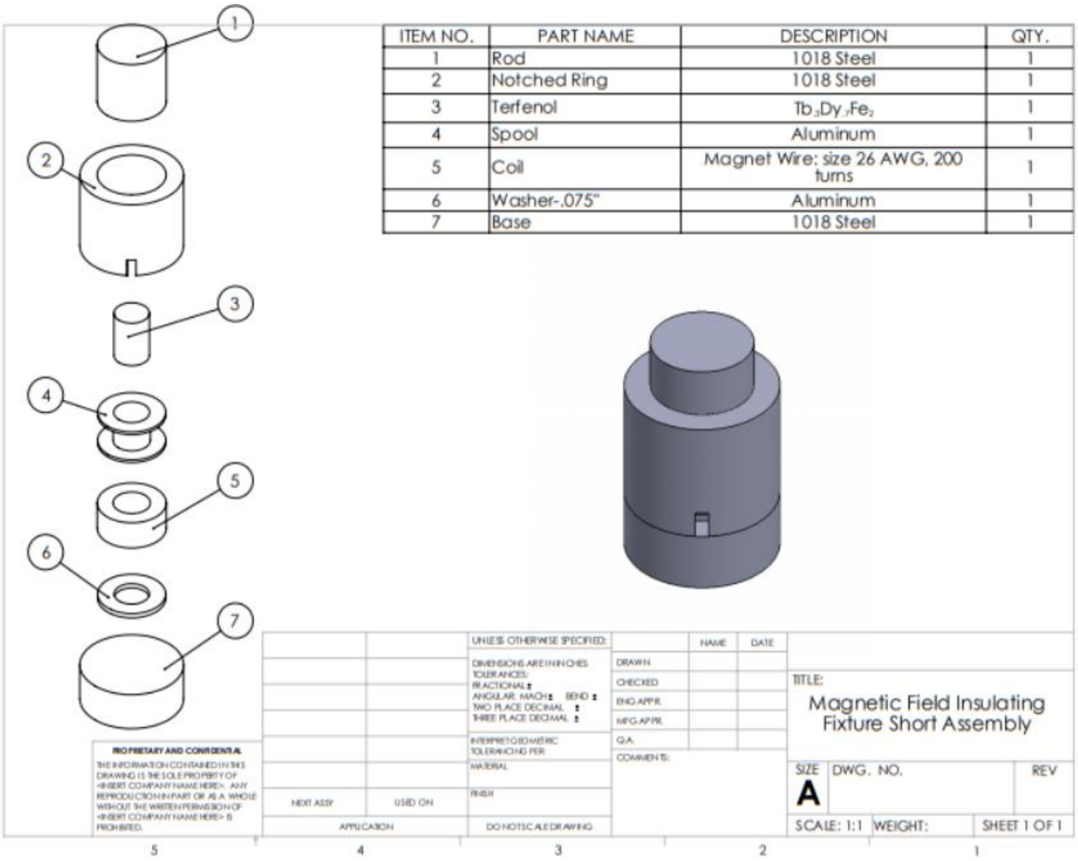

ITEM NO.	PART NAME	DESCRIPTION	QTY.
1	Rod	1018 Steel	1
2	Notched Ring	1018 Steel	1
3	Terfenol	$Tb_{.3}Dy_{.7}Fe_2$	1
4	Spool	Aluminum	1
5	Coil	Magnet Wire: size 26 AWG, 200 turns	1
6	Washer-.075"	Aluminum	1
7	Base	1018 Steel	1

Figure 3. Terfenol-D test fixture [11]

The Terfenol-D based harvester was placed on a Material Testing System (MTS) machine which can simulate the cyclic loading bearings endure on a railcar. Although Estrada’s energy harvester could generate a significant amount of energy, the device could only be optimized as either an energy harvester or a load sensor. Utilizing the knowledge gained from Estrada's results, Bensen [12] commenced work aimed at developing a Terfenol-D based energy harvester. Bensen's energy harvesting device was downscaled and modified to fit on a bearing adapter. In Bensen's design, four coils were placed in the highest-pressure points of the adapter to capture the highest contact forces during operation. However, Bensen concluded that each cylinder was only able to produce an estimated 36.3 μW with a max instantaneous power of 0.53 mW. Moreover, the design was not rugged enough to withstand the harsh environments seen in freight railcar service.

1.4.2 Piezoelectric Energy Harvesting

Other vibration-based energy harvesting devices include the use of piezoelectric materials. These materials use the piezoelectric effect to generate electricity from mechanical strain. The mechanical strain can be generated from a variety of sources such as low-frequency seismic vibrations, acoustic noise, and even human motion. Piezoelectric energy harvesting has been implemented in a wide range of applications, spanning from consumer products to industrial use. Although piezoelectric-based energy harvesting devices have been implemented in the rail industry, they are mostly used on the track's wayside. Mishra, *et al* [13] embedded two different piezoelectric systems (compression type and cantilever-beam type) in the railway track to determine their power output. In their study, they concluded that the harvesters were able to generate enough energy to operate signal signs and lights in remote areas.

1.4.3 Solar Energy Harvesting

The improvement in solar panels in recent years have shown great potential in the amount of energy they are able to produce in freight applications. Solar panels are made of photovoltaic cells that use solar radiation to generate electricity. These photovoltaic (PV) cells contain layers of semiconductor material that contain differing quantity of electrons. When PV cells are stacked, a positive-negative (p-n) junction is formed that initiates an electron flow the instant light from the sun hits the junction. Vasisht *et al* [14], conducted a study on photovoltaic systems on train rooftops. From their research, they found that their “SPV coach”, a photovoltaic cell fitted freight car, was able to produce around 1.3 kWh per day which is more than sufficient to operate low power electronic circuits.

1.4.4 Thermoelectric Energy Harvesting

Thermoelectric generators (TEGs) work by turning a heat source into electricity. This is accomplished using the Seebeck effect, a phenomenon where a voltage is produced by having a temperature gradient between two surfaces that are connected by a positive (p) and negative (n) semiconductor. Both surfaces are made of a ceramic substrate and are separated into a “hot” side and a “cold” side. When a temperature difference between both ceramic surfaces is present, the heat is transferred from the hot side of the TEG to the cold side. Due to the differing electron density of the semiconductors, the charge begins to move through its respective semiconductor creating a voltage potential. Because the semiconductors are connected in series, the voltage potential is added across the entire module. Ahn and Choi [15] used thermoelectric modules to harvest ambient energy generated from a rolling stock bearing housing on a high-speed train. From the data gathered in their experiment, using the open circuit voltage of a single thermoelectric module, they were able to obtain around 19.2 mW of power [15].

1.5 Energy Harvesting Technique Selection

The selected energy harvesting technique must follow the following criteria to be considered as a promising energy harvesting solution for this engineering application. First, the harvesting technique must not be highly dependent on external weather conditions. Second, the harvesting technique must lend itself to be universally fitted on multiple railcar designs. Third, the energy harvesting device must be resilient enough to withstand the harsh conditions and long mileage that freight railcars endure.

Vibration-based energy harvesting devices meet the first two criteria by being modular enough to fit on most railcars while also having their performance be independent from external weather conditions. Due to their composition of brittle materials, the main concern with this type of energy harvesters is their ruggedness in being able to withstand the high mileage railcars see in service. Bensen's energy harvester was not able to withstand the cyclic loading during testing and concluded that the magnets used were not robust enough for rail industry use. PV panels only meet one criterion in which they are resilient enough to withstand the high mileage railcars experience. Otherwise, PV cells fail to meet the first two criteria which are arguably the most important of the three. First, their performance is dependent on the sun exposure time available during the trip and cannot generate as much energy in cloudy conditions or at night. Second, PV panels require a large surface area which makes them less compatible with railcars that have an open container design, thus, limiting their universal fitting.

Thermoelectricity is the harvesting technique that best fits all the criteria from the methods discussed. First, their solid-state design makes them advantageous for this application as they suffer minimal wear from railcar vibrations. Second, they can be affixed to any bearing adapter, making them universally compatible with any freight railcar design. Last, they can operate under any weather conditions and remain operational as long as a temperature difference exists between the ambient and the bearing operating temperature. Although previous research has been conducted on TEGs mounted to high-speed passenger trains, this study hopes to contribute to the earlier work by developing a complete energy harvesting device with the required circuitry needed to charge an energy storage element for freight transportation use. The performance of the harvesting device will be validated using a dynamic bearing test rig that can mimic field operating conditions using a simulated test plan based on common freight routes. The harvesting device will simultaneously charge a battery while it powers a wireless onboard bearing health monitoring device that will be executing an algorithm like the one designed for field service implementation.

CHAPTER II

DESIGN CONSIDERATIONS

2.1 Thermoelectric Generators and Cooling Solution

2.1.1 Thermoelectric Generator Models

The amount of energy collected by a thermoelectric generator (TEG) will be entirely dependent on the temperature gradient across both faces of the TEG. Two types of TEGs were used in this study which include the Tecteg TEG1-1263-4.3 (30×30 mm) and the Tecteg TEG2-126LDT (40×40 mm) scavenger model. Although both TEGs use Bi_3Te_3 (Bismuth telluride) semiconductors, their optimal performance differs in the magnitude of the temperature gradient. This means the TEG2-126LDT models are designed to work best with smaller temperature gradients contrary to the TEG1-1236-4.3 model which are designed to work best at larger temperature gradients. Although the larger surface area of the TEG2-126LDT might seem like the clear choice for this application, the smaller footprint of the TEG1-1236-4.3 can increase the harvesting capacity by permitting additional units in tighter spaces. Due to the complex shape of the bearing adapters, the TEGs need to be placed in an area that provides both a good surface contact with the heat source and a high surface temperature.

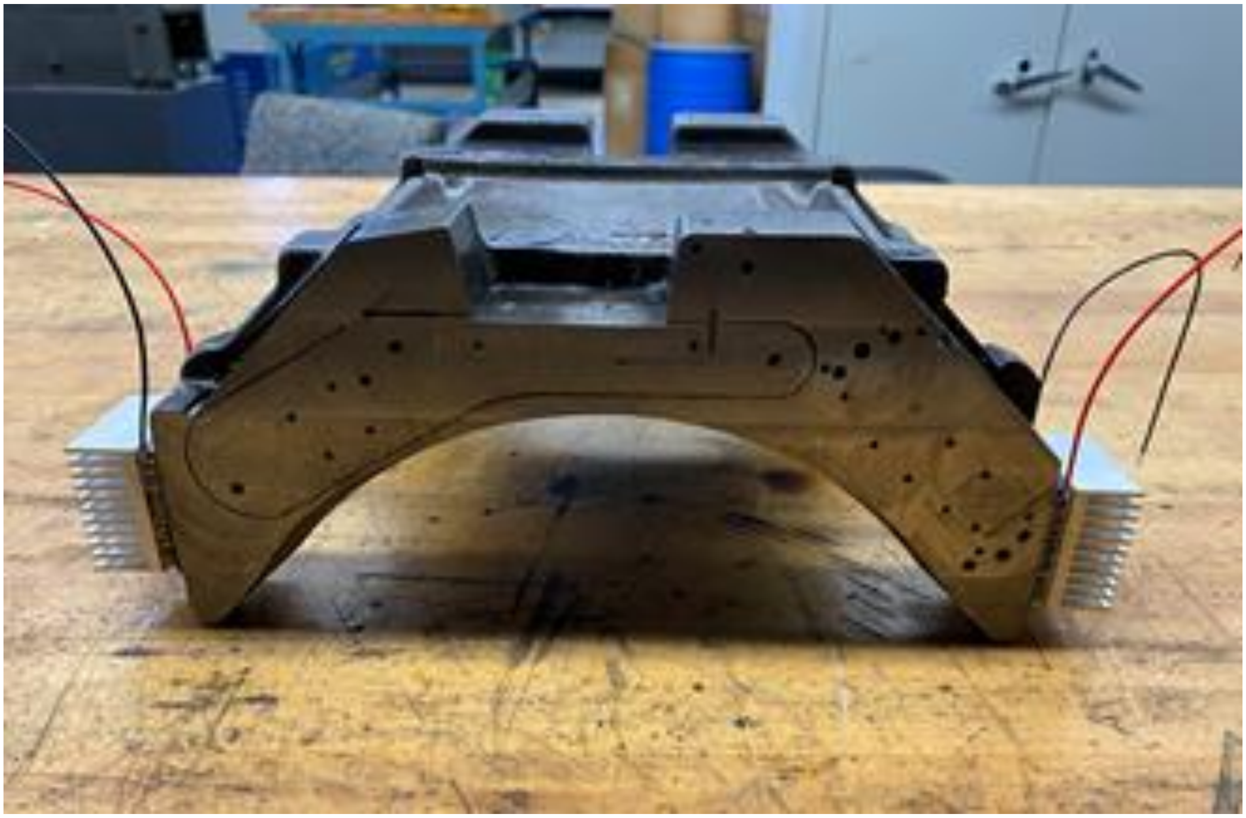

Figure 4. TEG/Heat sinks mounted on the bearing adapter

As pictured in Figure 4, the TEGs were placed on the vertical leading and trailing surfaces of the bearing adapter to ensure maximum surface contact area between the TEG and the adapter. Additionally, this location also provides the highest surface temperature aside from the bearing itself. Note that the bearing outer ring (cup) indexes in field service operation which excludes anything from being affixed to the outside cup surface.

2.1.2 Heat Sink Design

The heat sinks used are made of 6063-T5 aluminum that have a thermal conductivity of 201 $\frac{W}{m \cdot k}$. These heat sinks are used to dissipate the heat from the TEG via forced convection generated by the airstream as the train travels down the track. By having two TEGs mounted on both sides of the adapter, the energy harvesting device can provide optimal performance regardless of the train's direction of travel. The thermal resistance of the 30×30 mm and 40×40 mm TEG is 0.5 $\frac{K}{W}$ and 1.5 $\frac{K}{W}$, respectively.

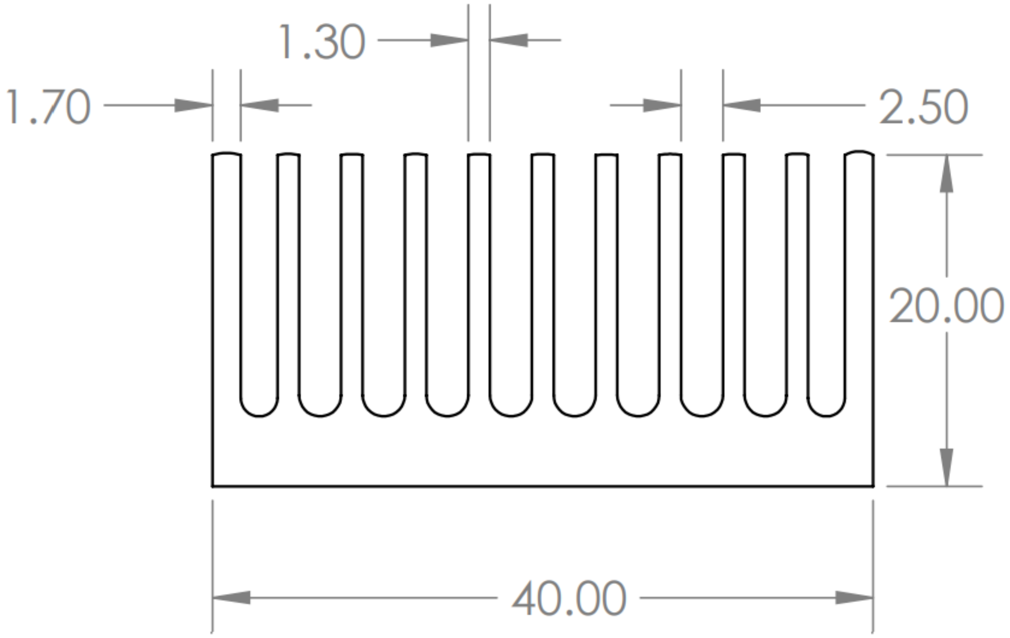

Figure 5. 40×40 mm heat sink schematic (dimensions in millimeters)

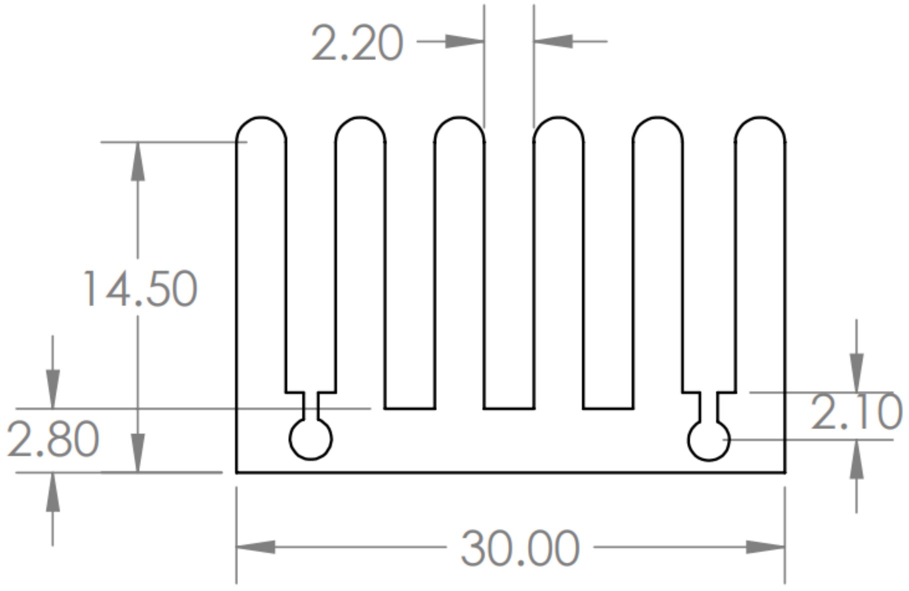

Figure 6. 30×30 mm heat sink schematic (dimensions in millimeters)

The TEGs and heat sinks were mounted to the adapter using a thermal adhesive that has a thermal conductivity value of 0.9 $\frac{W}{mk}$. The thermal adhesive helps fill in the microscopic air pockets present in the rough surface finish of the cast steel bearing adapter. By filling the voids, heat transfer is increased thus directly increasing the power generated by the TEGs. Both TEG models have a thin graphite layer that, with a pressure mounting system, will mold to the adjacent surface to improve the surface contact area between both components. Although the TEGs are manufactured with the graphite layer, the thermal adhesive is used as a temporary mounting solution and is meant exclusively for laboratory experimentation.

2.2 Energy Harvester Components

The TEG devices are only a single element of the complete energy harvesting system design. The energy harvester must also include the appropriate components and circuitry needed to manage and charge an energy storing device since the power source is intermittent. Figure 7 shows the block diagram for the wiring of the components used. The complete energy harvesting device is composed of TEGs, heat sinks, boost converter, and a battery management chip (BMC). All parts in this design are commercially available components which help improve cost and modularity of components. The block diagram also includes the components the energy harvesting device will supply power to, which include the wireless condition monitoring device and the battery.

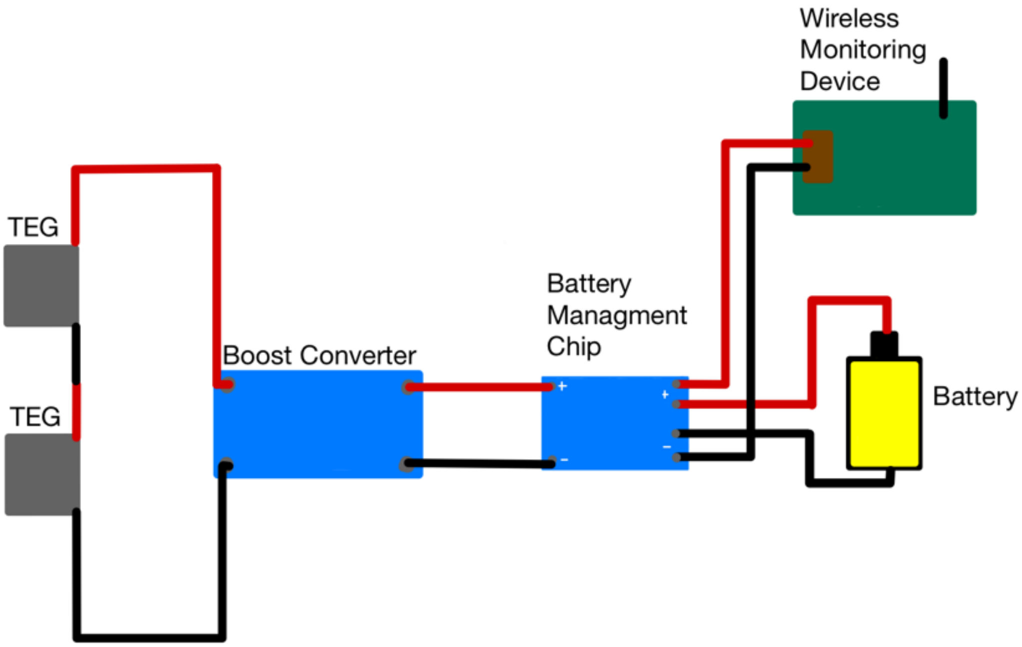

Figure 7. Block diagram of the energy harvesting device

2.2.1 Energy Storing Element Selection

A 14500 lithium-ion battery was selected as the energy storage element for this application as it can provide the appropriate voltage needed for the wireless monitoring device to function. Lithium-ion batteries provide several benefits when compared to traditional cell technologies. First, the 14500 batteries selected provide a voltage of 3.7-volts per cell in contrast to traditional alkaline batteries which only provide 1.5-volts per cell. This results in fewer batteries needed to operate the wireless monitoring device, thus reducing the size, weight, and cost of the device. Second, lithium-ion batteries exhibit a flatter discharge curve compared to their carbon-zinc and alkaline counterparts, as demonstrated in Figure 8. This allows the lithium-ion batteries to hold the required voltage for a larger portion of the State of Charge (SoC).

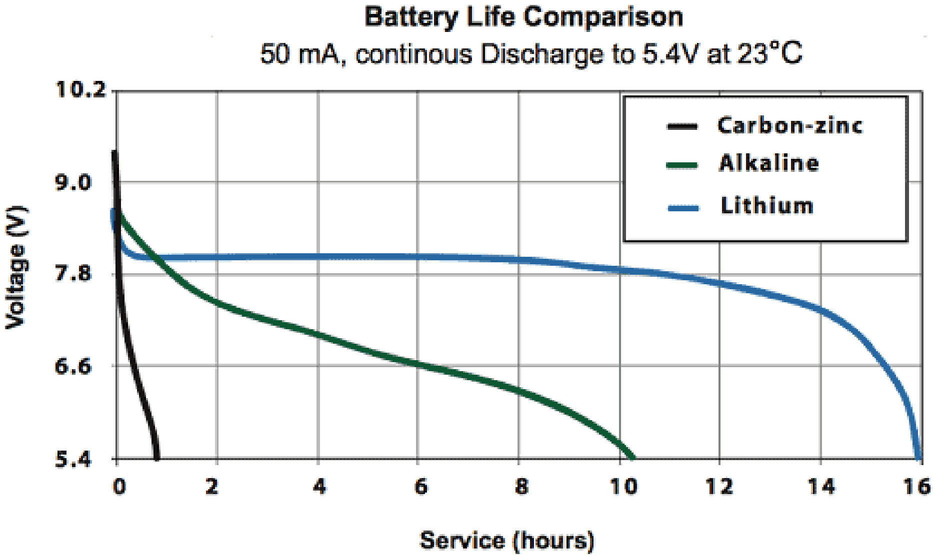

Figure 8. Discharge rate of different battery technologies [16]

2.2.2 Energy Harvester Electrical Components

The TEGs were wired in series to ensure a maximum output voltage. The output voltage feeds into the boost converter which operates at a minimum input voltage of 0.9-volts and boost the voltage to 5-volts. The boost converter's output then feeds into the input of the battery management chip (BMC) which uses a TP4056 chip that regulates the voltage and current needed to charge the lithium-ion battery. The TP4056 chip offers overcharge protection to stop any damage from occurring to the battery in a scenario where the TEG and boost converter are producing available power, but the battery is fully charge. The charging cycle behavior for a 1000 mAh battery was obtained from the manufacturer's specification sheets and is shown in Figure 9. The output of the BMC is connected to the electrical load, in this case the wireless monitoring device, and the lithium-ion battery. This allows for the battery to power the wireless monitoring device while the energy harvesting system charges the battery when there is a sufficient temperature gradient present. If the TEGs are not able to produce the voltage required start the boost converter, the wireless monitoring device will run on the battery alone.

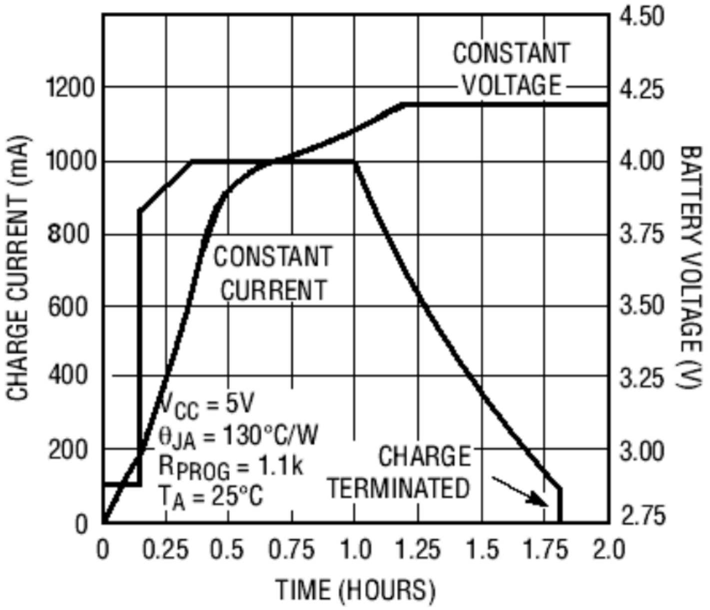

Figure 9. TP4056 charge cycle [17]

2.2.3 Other Electrical Components

Figure 10 shows the LTC 4150 coulomb counter operated by an Arduino Uno board used keep track of the charge going in and out of the battery during the laboratory experiments. Since these components were used solely for experimental purposes and would not be part of the field-implementation system, they were powered by a separate power source which is excluded from the data presented in the following sections.

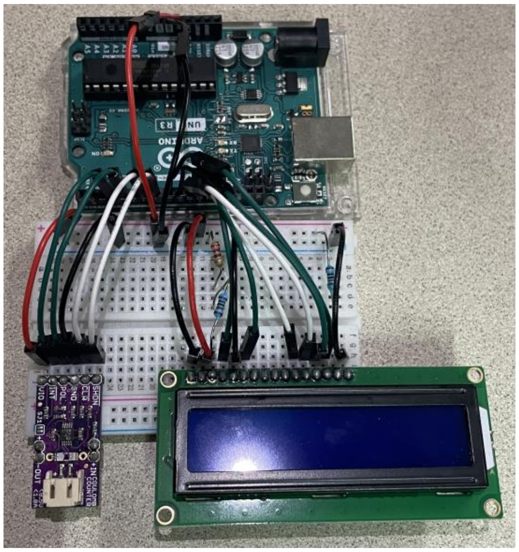

Figure 10. Coulomb counter and Arduino setup

2.3 TEG Optimization

To determine the maximum power point (MPP) of the TEG, a hot plate and heat sink/cooling fan were used as a heating and cooling source for the TEG (Figure 11). Once a thermal steady state was reached, a resistor was connected to the output of the TEG to determine the amount of voltage and current produced. After the values were recorded for the corresponding resistor, the process was repeated with a different resistor value. This experimental process was carried out for both TEG models using resistor values of 1, 2, 5.1, 10, 16, 51, 63, 75, 100, 150, and 200 Ω.

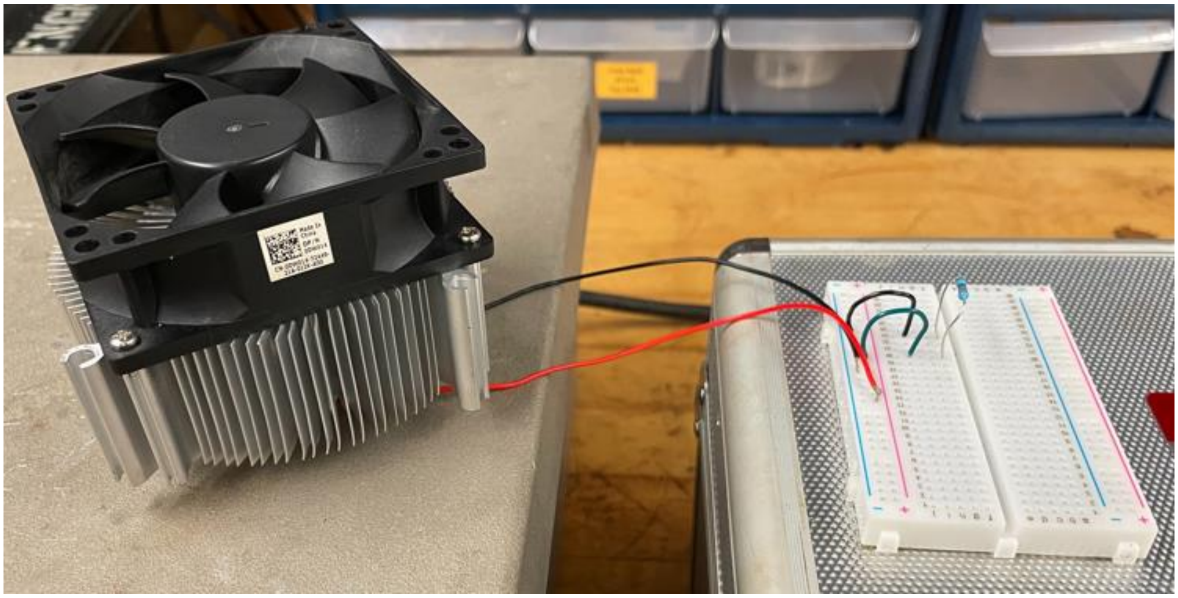

Figure 11. TEG optimization setup

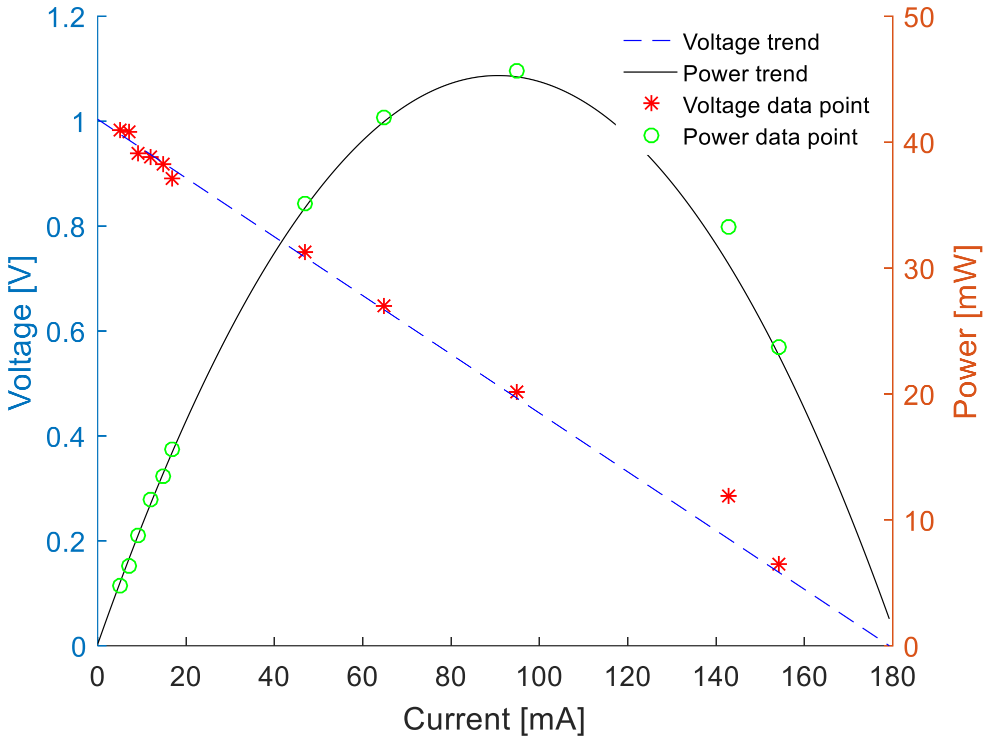

Figure 12. Thermoelectric performance of TEG2-126LDT (40×40 mm)

Figure 12 displays the voltage and current that were acquired from testing the set of resistors listed previously. A linear trend was obtained to determine the Open Circuit Voltage (V_{oc}) and the Short Circuit Current (I_{sc}). The open circuit voltage is the point at which the voltage is highest and there is no current flowing. In contrast, the short circuit current is the point at which the current is highest while there is no voltage produced. These values can yield the optimal power (P_{opt}) and the optimal load resistance (R_{opt}) by using Equation (1) and (2).

$$P_{opt} = \frac{V_{oc} \cdot I_{sc}}{4} \tag{1}$$

$$R_{opt} = \frac{V_{oc}}{I_{sc}} \tag{2}$$

For the TEG2-126LDT, a V_{oc} value of 1 V and I_{sc} value of 179.47 mA were determined from Figure 12. Inputting these values into Equation (1) and (2) yielded an optimal power and an optimal resistance of 44.87 mW and 5.57 Ω, respectively. Equation (1) reflects the fact that the maximum power occurs at the midpoint of the line connecting the V_{oc} and I_{sc} in Figure 12. At this point the voltage is $V = \frac{V_{oc}}{2}$, while the current is $I = \frac{I_{sc}}{2}$, and therefore the power $P = V{\cdot}I$ is given in Equation (1). A polynomial trend was then obtained from the power values derived from the voltage and current data points. By looking at the polynomial power trend, the highest value seen was 45.28 mW, which closely matches (~1%) the theoretical optimum value of 44.78 mW.

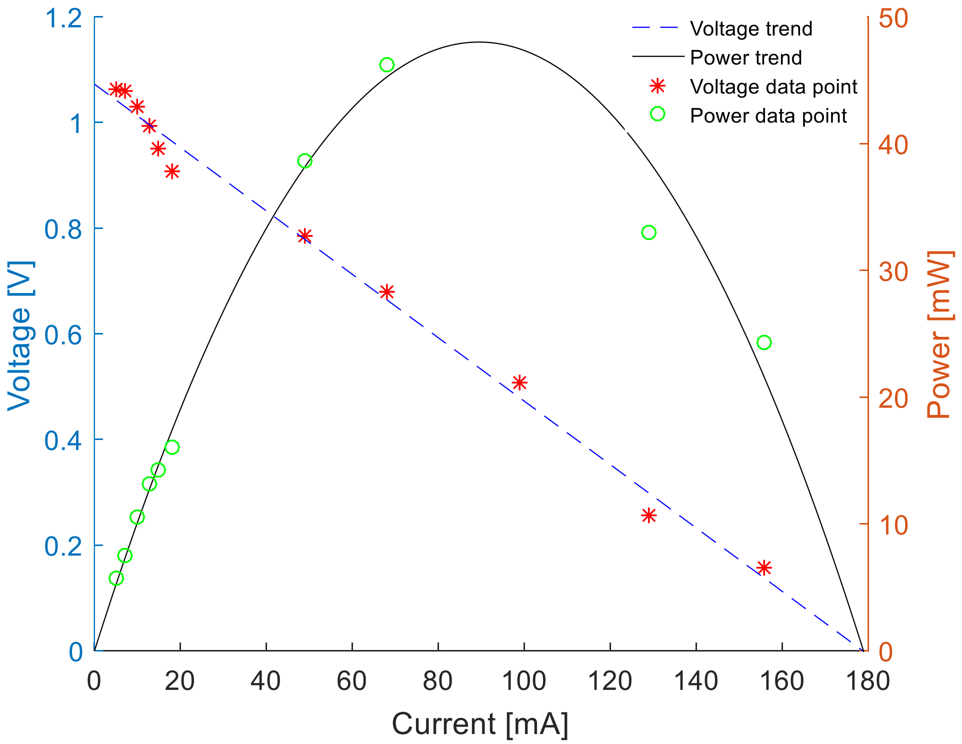

Figure 13. Thermoelectric performance of TEG1-1263-4.3(30×30 mm)

The process was repeated for the TEG1-1263-4.3 (30×30 mm) using the same resistor values. The V_{oc} and I_{sc} was determined to be 1.07 V and 178.73 mA from Figure 13. These values resulted in an optimal power and an optimal load resistance of 47.81 mW and 5.99 Ω, respectively. With the corresponding voltage and current data points, the power values were then obtained and used to derive the polynomial power trend. The MPP value for the smaller TEG was determined to be 48 mW which closely matches the theoretically acquired optimal power value.

2.4 TEG and Boost Converter Optimization

To optimize the performance of the TEG and boost converter working in tandem, a TEG was used as a voltage source using the same hot plate and heat sink/cooling fan combination. The output of the TEG was connected to the boost converter input while a resistor was placed at the output of the boost converter to act as a load for the setup as depicted in Figure 14. A sufficient temperature gradient was generated for the TEG to produce an output voltage of 1 V, which is the minimum voltage required for the boost converter to function. Once a thermal steady state was achieved, the voltage across the resistor was acquired for a series of resistor values. The purpose of this optimization exercise was to determine the smallest resistance value that will allow the boost converter to produce the 5-volt output.

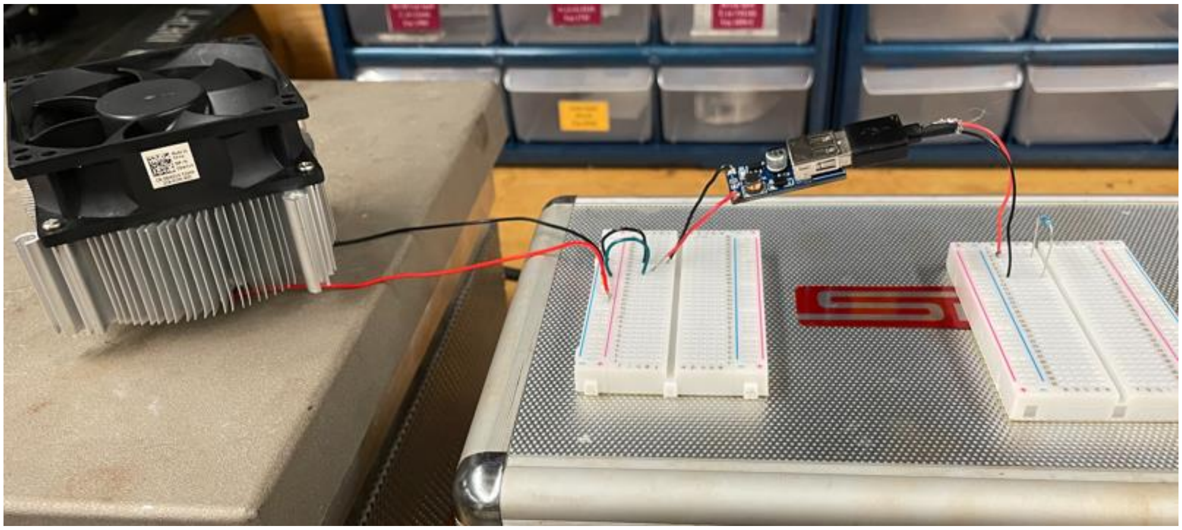

Figure 14. TEG and boost converter optimization setup

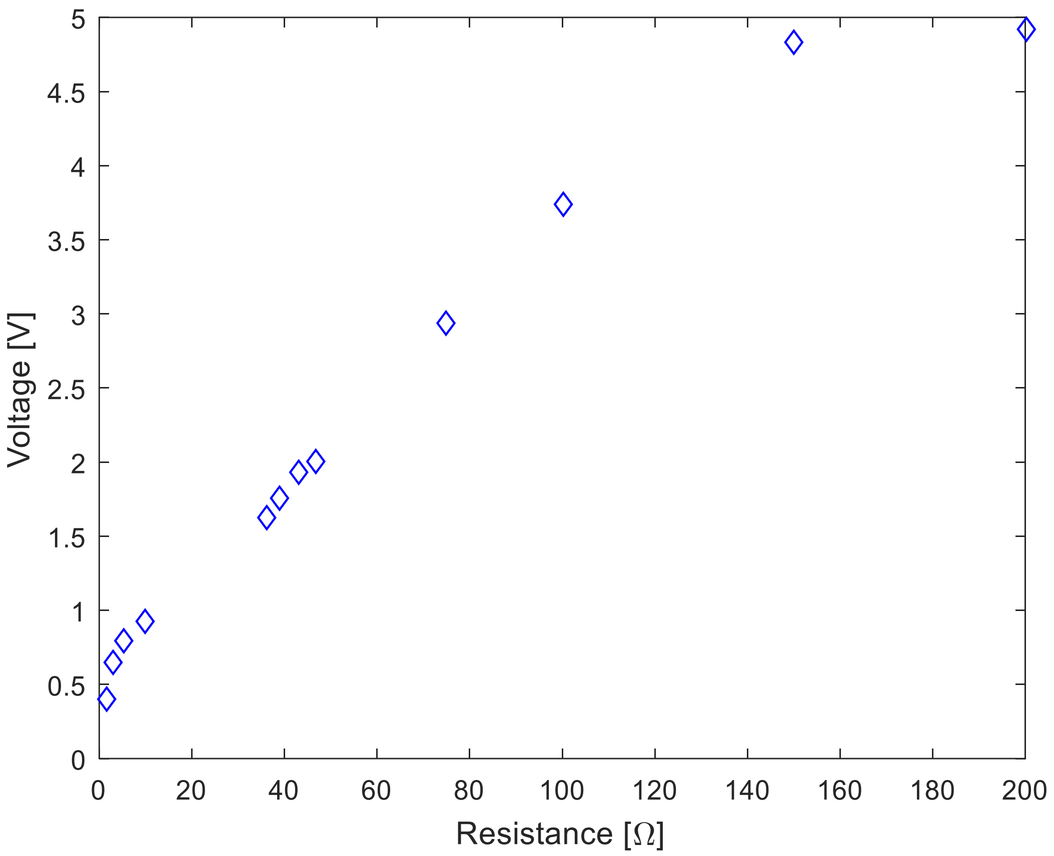

Figure 15. Voltage produced at various resistances using TEG2-126LDT/boost converter

Table 1. Voltage and Current values for TEG2-126LDT/boost converter

Resistor [Ω]	Voltage [V]	Current [mA]
1.5	0.40	268.7
3	0.66	218.3
5.1	0.80	156.9
10	0.92	92.2
36	1.62	45.1
43	1.93	44.8
47	2.01	42.8
75	2.94	39.1
100	3.75	37.5
150	4.84	32.2
200	4.92	24.6

The data in Table 1 presents the voltages produced using a combination of the boost converter and TEG2-126LDT (40×40 mm) at different load resistances. In this data set, the resistance values of 150 Ω and 200 Ω resulted in voltages that were close to the target 5-volts.

Although the 200 Ω resistor was closer to the desired 5 V, the boost converter current was 24.6 mA, whereas at 150 Ω, the boost converter current was at the higher value of 32.2 mA.

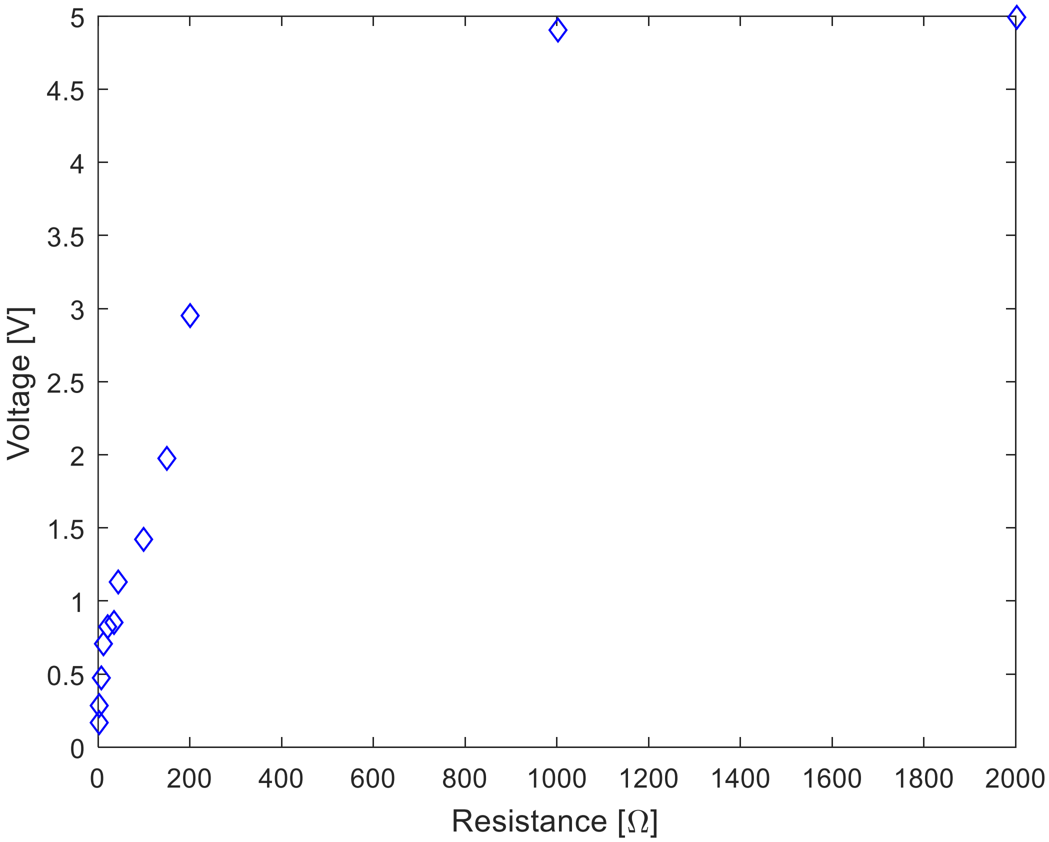

Figure 16. Voltage produced at various resistances using TEG1-1263-4.3/boost converter

Table 2. Voltage and current values for TEG1-1263-4.3/boost converter

Resistor [Ω]	Voltage [V]	Current [mA]
1.5	0.16	109.3
3	0.29	96.3
5.1	0.48	93.5
10	0.71	71.1
36	0.86	23.8
43	1.13	26.3
100	1.42	14.2
150	1.98	13.2
200	2.95	14.8
1000	4.91	4.9
2000	5.00	2.5

Table 2 presents the results for the same experimental procedure for the TEG1-1263-4.3 (30×30 mm). In this data set, the resistance values of 1 kΩ and 2 kΩ were the closest resistances to producing the 5-volts needed. Similar to previous results, although 2 kΩ reached closer to the 5-volt minimum it only produced 2.5 mA while 1 kΩ produced double the current at 4.9 mA.

The experiments just described gave the maximum current that can be drawn from the boost converter output. The next step in the design was to adjust the battery management circuit so that it draws approximately this much current. The battery management circuit used here allows resistor programmable control of the battery charging current I_{bat} using the following equation:

$$I_{bat} = \frac{V_{Prog}}{R_{Prog}} \times 1200 \tag{3}$$

Where R_{prog} is a programming resistor within the battery management circuit. Equation (3) is obtained from the specification sheets of the BMC manufacture [17]. Although the battery charge current and input current drawn from the boost convertor are not precisely identical, they are comparable, so that we can set the charge current I_{bat} close to the optimum boost convertor output current determined from Figure 15 and Figure 16. Equation (3) was then used to obtain the R_{prog} value needed for the BMC to work at optimum performance. For this BMC the manufacture states a V_{prog} value of 1-volt. The data collected in these tests yielded a R_{prog} value of 37 kΩ for TEG2-126LDT and 244 kΩ for TEG1-126-4.3.

CHAPTER III

EXPERIMENTAL SETUP AND PROCEDURES

3.1 Route Simulation Selection

To verify the performance of the TEG-based energy harvesting device, a prototype unit was mounted on one of the UTCRS dynamic bearing test rigs described in Section 3.2. A set of test plans were developed to mimic the operating conditions seen in common freight routes. The first route selected was between Billings, MT and Council Bluffs, IA. This route is commonly used to transport coal and is approximately 896.4 miles in length and takes about 15.76 hours to complete. The second route selected was between Fairfield, AL and New Orleans, LA. This route simulates a railcar transporting cargo from a steel mill to a shipyard. It runs 427.2 miles in length and takes approximately 11.59 hours to complete. The speeds in the test plans were estimated by using the urban density of a corresponding area along with existing railroad speed data[18]. Figure 17 and Figure 18 show the maps for these two routes. Table 3 and Table 4 list the cities these routes intersect along with the distance between the cities, the simulated train speed, and the time elapsed between the train leaving one city and reaching the next at that speed.

Figure 17. Map of Route 1 (Council Bluffs, IA - Billings, MT) [19]

Table 3. Distance and speed limits of Route 1 (Council Bluffs, IA - Billings, MT)

City	Distance [mi]	Speed [mph]	Elapsed Time [h]
Council Bluffs	0.0	25	0.97
Gretna	24.3	35	0.30
Ashland	34.8	60	9.83
Moorcroft	624.6	53	0.25
Rozet	637.8	45	0.40
Sheridan	655.8	60	4.01
Billings	896.4	60	0.00

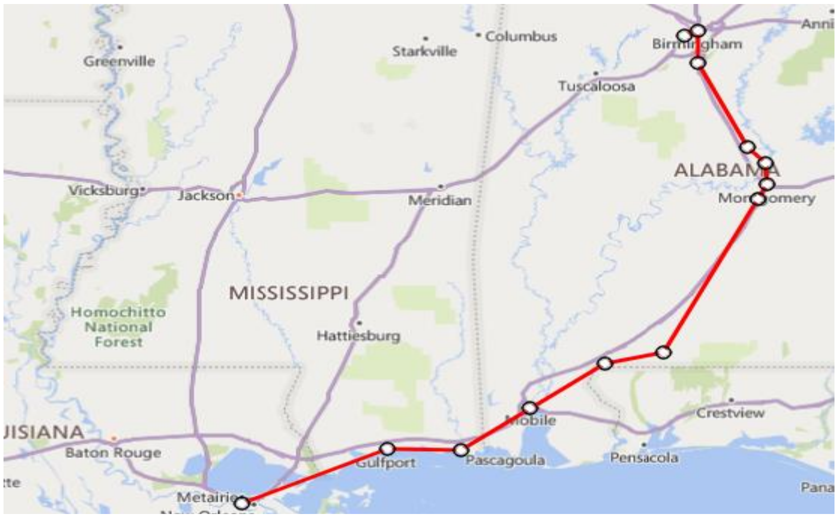

Figure 18. Map of route 2 (Fairfield, AL – New Orleans, LA) [19]

Table 4. Distance and speed limits of Route 2 (Fairfield, AL – New Orleans, LA)

City	Distance [mi]	Speed [mph]	Elapsed Time [h]
Fairfield	0.0	25	1.26
Pelham	31.5	35	1.52
Rollins	84.7	55	0.22
Elmore	96.8	35	0.33
Montgomery	108.4	25	0.36
McGehees	117.4	60	1.61
Brewton	214	55	0.51
Atmore	242.0	45	0.98
Mobile	286.1	35	2.11
Gulfport	360	25	2.69
New Orleans	427.2	25	0.00

The two routes were used to quantify the performance of the energy harvester in a worst- and best-case scenarios. Route 1 is in a rural area which allows the train to travel at higher speeds for longer periods of time, while Route 2 is in an urban location that requires the train to travel at lower speeds for shorter periods of time. The route simulation experiments in this study were conducted in two segments. The first segment simulated the railcar traveling to its destination fully loaded, while the second segment simulated the railcar traveling empty to its initial point of origin. During each trip, the accumulated charge for the corresponding speed was used to acquire the average current and power produced. The objective of these experiments was to determine if the amount of charge produced by the temperature difference between the ambient and the bearing adapter is sufficient to increase the charge of the battery while simultaneously powering the wireless condition monitoring device.

3.2 Dynamic Bearing Test Rigs

All experiments for this study were conducted using the dynamic bearing test rigs built by the research team at the University Transportation Center for Railway Safety (UTCRS). These test rigs include the Single Bearing Tester (SBT), pictured in Figure 19, the 4-Bearing

Tester (4BT), seen in Figure 20 (left), and the 4-Bearing Chamber tester (4BCT), shown in Figure 20 (right).

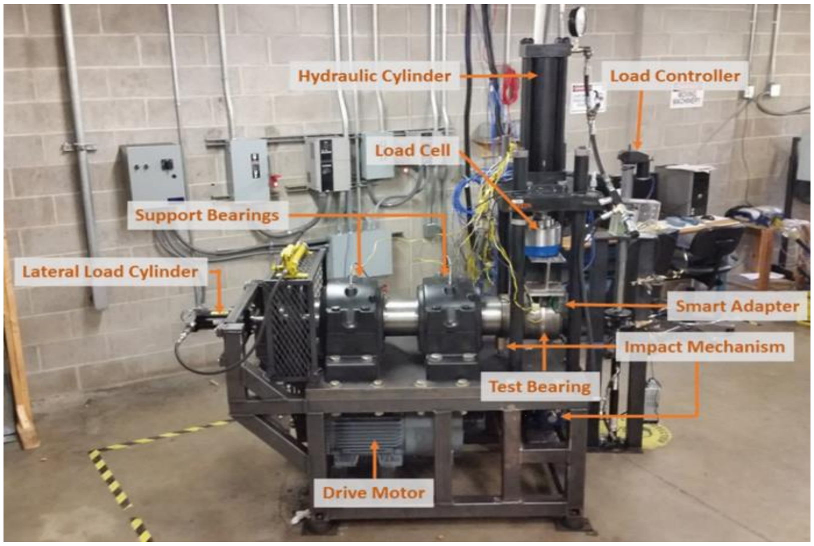

Figure 19. Single Bearing Tester (SBT)

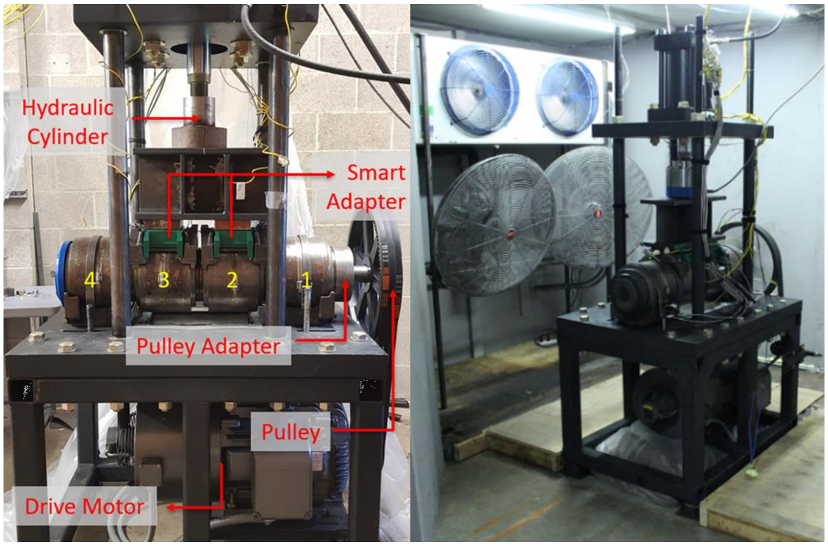

Figure 20. 4-Bearing Tester (Left) and 4-Bearing Chamber Tester (Right)

The testers are uniquely designed to mimic the operating conditions of class K (6½"×9"), class F (6½"×12"), class G (7"×12"), and class E (6"×11") tapered roller bearings in freight rail service. For this particular study, only class F and class K bearings were used in the experiments. The bearings were subjected to two loading conditions which include 17% railcar load (i.e., a load of 26 kN or 5.85 kips per bearing), representing an empty railcar, and 100% railcar load (i.e., a load of 153 kN or 34.4 kip per bearing), replicating a fully loaded railcar. The simulated load is achieved by utilizing a hydraulic cylinder that can apply loads of 150% of the full load seen by class F and K bearings in service. Arduino based load controllers are used to maintain a constant applied load on the bearings and automatically adjust the load to counteract any load variations that occur during testing due to thermal expansion and contraction effects of the hydraulic oil. The tester is also fitted with a 22 kW (30 hp) variable frequency motor that allows the tester to achieve speeds up to 137 km/h (85 mph). Industrial fans are set perpendicular to the tester to provide passive air cooling (6 m/s or 13.4 mph) to the bearings. The SBT accommodates a single railroad bearing that is pressure fitted onto a test axle that utilizes a cantilever-like setup similar to how the bearing is mounted on the wheel-axle assembly of a freight railcar. Contrary to the SBT, the 4BT and 4BCT can accommodate four bearings pressed onto a test axle. Although the 4BT and 4BCT test rigs can accommodate four bearings at a time, only data collected from the two middle bearings is taken into consideration because these two bearings are top-loaded, which is a realistic loading scenario, whereas the two outer bearings are bottom loaded and that is not typical of how these bearings are loaded in freight rail service. Finally, the only difference between the 4BT and the 4BCT is that the 4BCT is housed in a temperature-controlled environmental chamber that allows for the ambient to be maintained any temperature in the range from -40 to 65°C (-40 to 150°F).

3.3 Instrumentation and Data Acquisition

The data collected during these experiments were recorded using a LabVIEW^{TM} software package and a National Instruments (NI) NIcDAQ-9174 data acquisition system. All testers are strategically fitted with K-type thermocouples that monitor and record the laboratory ambient conditions, the bearing operating temperatures, and the corresponding bearing adapter temperatures. For these experiments, the thermocouple affixed to the bearing adapter, as depicted in Figure 21, was used to analyze the performance of the energy harvesting device. The thermocouples are connected to a NI 9213 card that collects data for half a second every twenty seconds at a sampling rate of 128 Hz. The energy harvesting voltages are obtained using a NI USB-6008 card which acquires the data at the same sampling rate used for the thermocouples. These sampling rates were selected to accommodate different experiments conducted simultaneously on the testers and are sufficient for analyzing the data acquired during testing performed for this study.

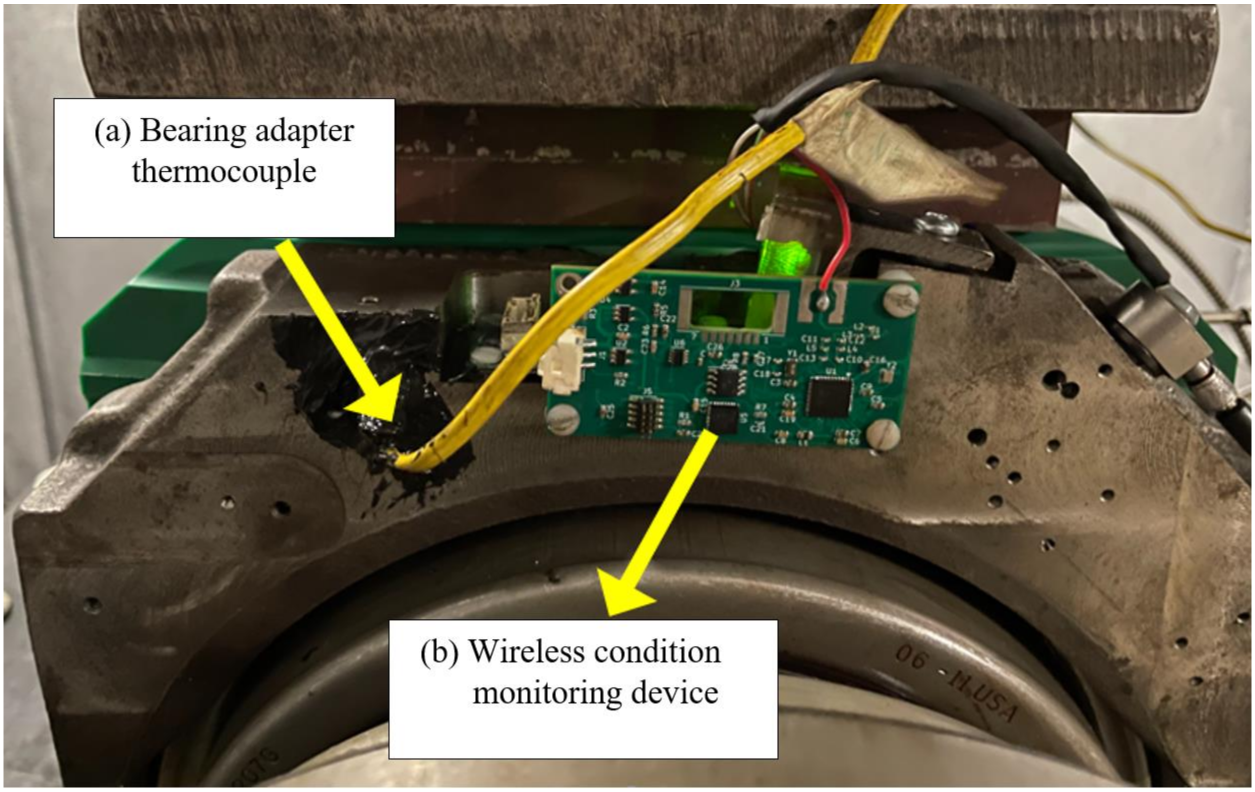

Figure 21. Picture showing (a) thermocouple placed in a groove in the bearing adapter and sealed to prevent outside air influence, and (b) wireless condition monitoring device

CHAPTER IV

DEVELOPMENT TESTING

4.1 TEG Performance on Bearing Adapter

Initial stages of experimentation featured two TEGs/heat sinks mounted to a bearing adapter on an operating test rig. This setup mimics field operating conditions and allowed the bearing adapter to reach operating temperatures like those seen in rail service. Hence, the bearing adapter acted as a heat source for the TEGs while the fans perpendicular to the tester provided a cooling source. The data acquired in these experiments was used to determine the theoretical maximum output of the TEGs. Therefore, the setup for these tests did not use the boost converter or the Battery Management Chip (BMC) to eliminate the losses introduced by these electronic components. The experiments were initialized once the testers reached steady state operating conditions to maintain consistency across the acquired results. A resistor was added to the output of the TEGs to obtain the voltage and current produced. The block diagram for the wiring of the test setup is provided in Figure 22.

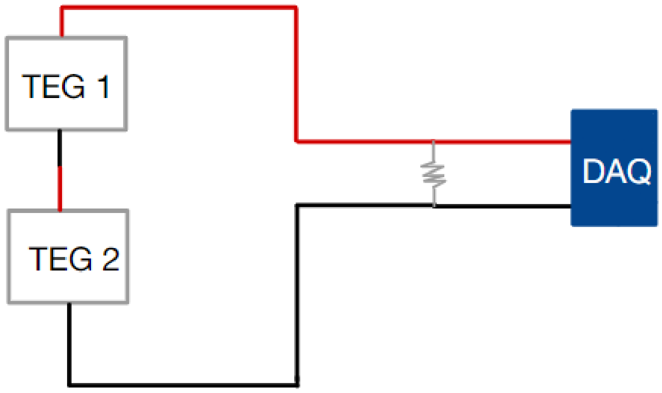

Figure 22. Block diagram of TEG devices wired in series with the data acquisition card

Preliminary testing was done using resistor values of 20, 46.6, 100, 150, and 200 Ω, but upon initial analysis of the data, it was deduced that additional set of resistor values were needed to find the optimal operating point. Hence, the tests were repeated using resistor values of 2, 5, 7, 10, and 15 Ω. The data gathered was used to generate plots that display the open circuit voltage (V_{oc}) and short circuit current (I_{sc}) that yield the optimal power and resistance using Equation (1) and (2) from Chapter II. Since the overall efficacy of the energy harvesting device was being assessed, the individual temperatures at each side of the thermoelectric generators were not used. Instead, the voltage generated by the TEGs was directly correlated with the temperature difference between the tester ambient conditions and the bearing adapter operating temperatures.

4.1.1 Experiment 228B (40×40 mm harvesters on bearing adapter)

Experiment 228B utilized two TEG2-126LDT energy harvesters wired in series on the Single Bearing Tester (SBT) bearing adapter. The experiment was first carried out at 17% railcar (simulating an empty railcar) with the motor set to 560 RPM, corresponding to a freight train traveling at 97 $\frac{km}{h}$ (60 mph). This is a common speed for freight trains traveling in rural areas, and closely replicates favorable conditions for the energy harvesting system. Figure 23 and Figure 24 show the temperature data collected (both ambient and adapter temperature) at the abovementioned operating conditions for resistor values of 2, 5, 7, 10, 15, 20, 46.6, 100, 150, and 200 Ω.

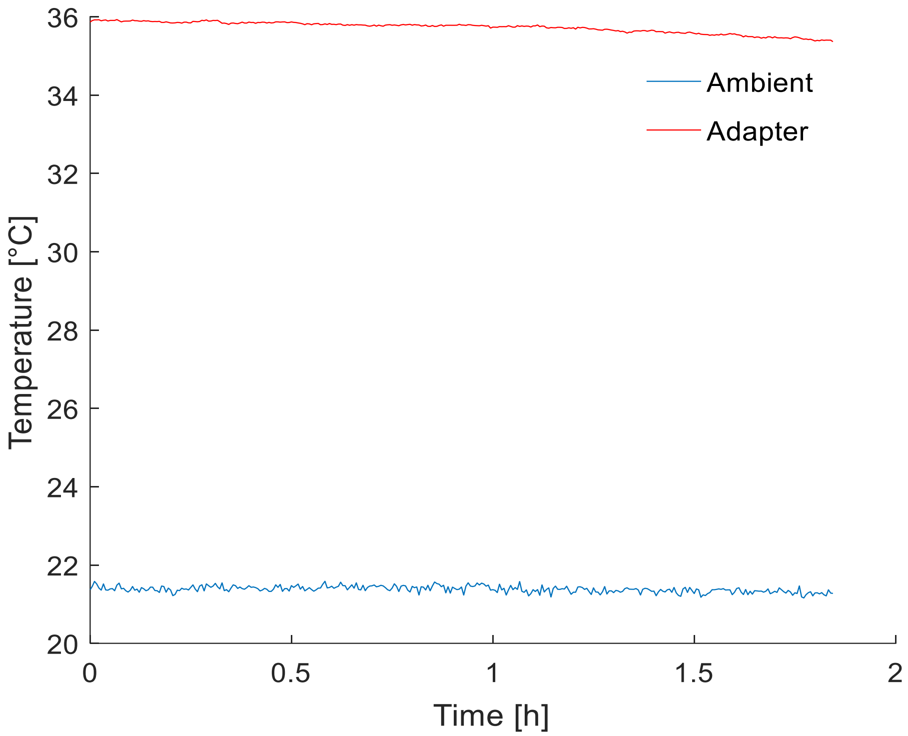

Figure 23. Experiment temperatures for 20,46.6,100, 150, and 200 Ω resistors at 17% load (empty railcar) and a simulated train speed of 97 km/h

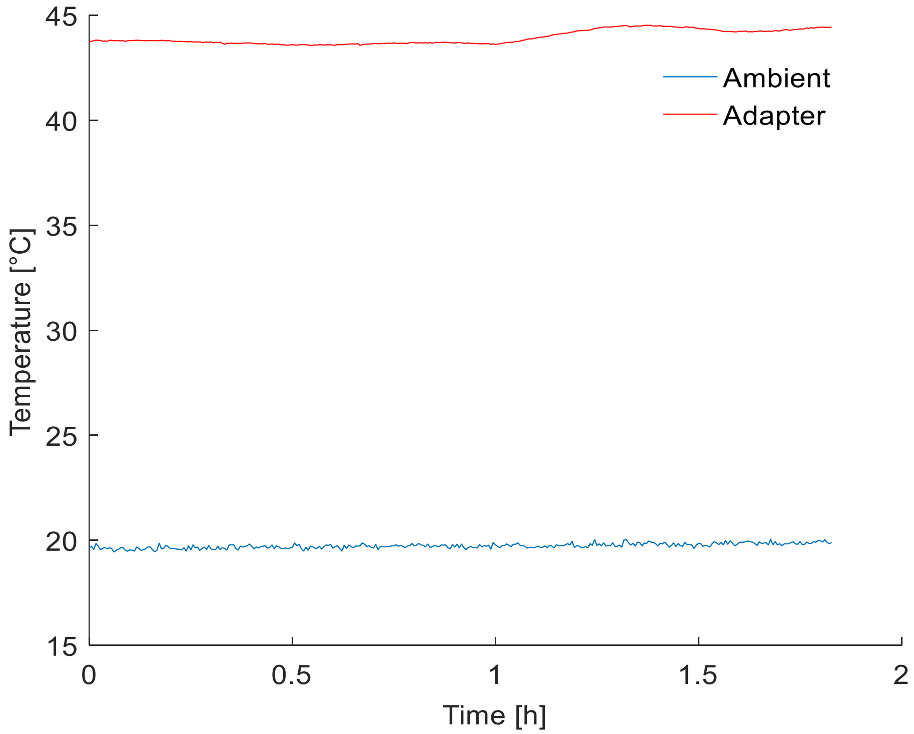

Figure 24. Experiment temperatures for 2, 5, 7, 10, and 15 Ω resistors at 17% load (empty railcar) and a simulated train speed of 97 km/h

Figure 23 displays the temperature data for the first set of resistors tested. For this data set, the ambient temperature of the laboratory remained constant at 21°C. Meanwhile, the adapter temperature averaged about 35°C resulting in a temperature difference of 14°C. For the data in Figure 24, the adapter operating temperature increased to an average value of 44°C whereas the ambient temperature of the laboratory was at 19°C, resulting in a temperature difference of 25°C. The voltages produced at 17% railcar load and a simulated train speed of 97 km/h can be seen in Figure 25 and Figure 26, respectively, for the two sets of resistors tested.

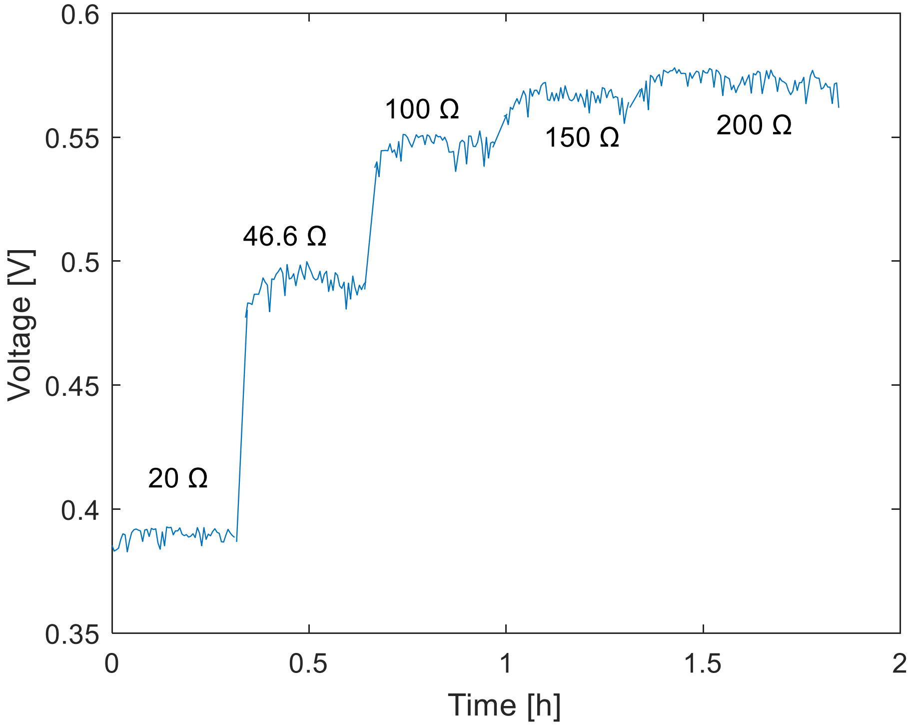

Figure 25. Voltages produced across 20, 46.6, 100, 150, and 200 Ω resistors at 17% load (empty railcar) and a simulated train speed of 97 km/h

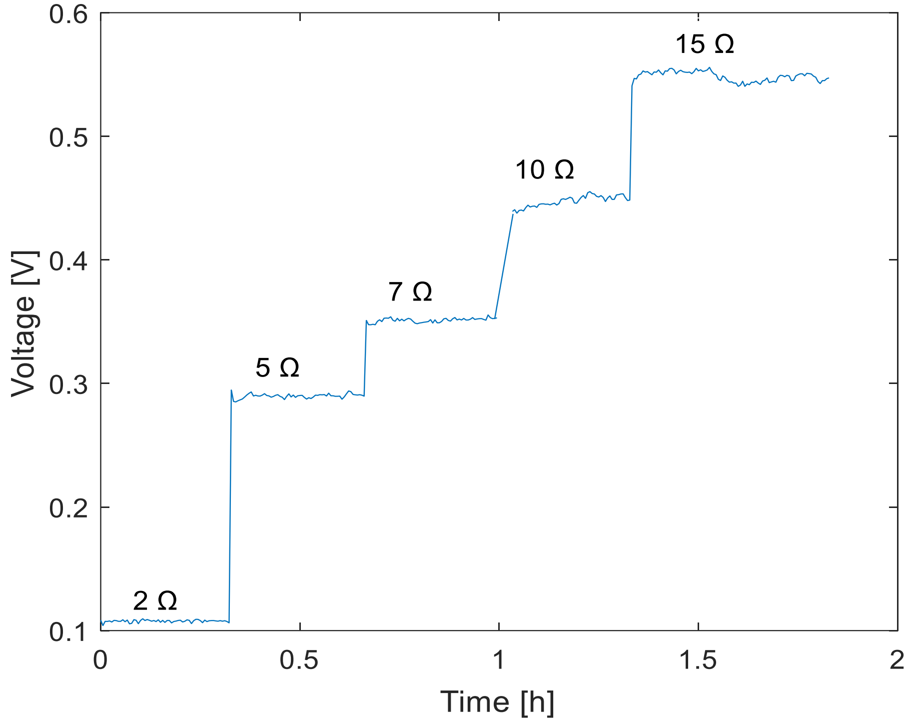

Figure 26. Voltages produced across 2, 5, 7, 10, and 15 Ω resistors at 17% load (empty railcar) and a simulated train speed of 97 km/h

Table 5 was produced by taking the average voltage of each resistor displayed in Figure 25 and Figure 26. From these data points, the mean current and power were derived for each resistor. These operating conditions produced the highest voltage value of 0.57 V at the resistor value of 200 Ω. Interestingly though this point also corresponded to the lowest power produced at 1.6 mW. The peak power output of 20.0 mW was produced at the two resistor values of 10 and 15 Ω. Regardless of load resistance, the voltage generated at this railcar load (i.e., empty railcar) is not sufficient to start the boost converter thus rendering the power produced by the TEGs useless as the battery management chip (BMC) will not be functioning. These results prompted the experiment to be repeated at 100% railcar load (full railcar). The temperature data for operating conditions corresponding to a fully-loaded railcar traveling at 97 km/h (60 mph) are displayed in Figure 27 and Figure 28, respectively, for the two sets of resistors tested.

Table 5. Average values for voltage, current, and power produced by the energy harvesters at the different resistor values while operating at 17% load (empty railcar) and a simulated train speed of 97 km/h

Resistance [Ω]	Average Voltage [V]	Average Current [mA]	Average Power [mW]
2	0.11	53.5	5.7
5	0.29	57.8	16.7
7	0.35	50.1	17.6
10	0.45	44.7	20.0
15	0.55	36.5	20.0
20	0.39	19.5	7.6
46.6	0.48	10.4	5.0
100	0.54	5.4	2.9
150	0.56	3.7	2.1
200	0.57	2.8	1.6

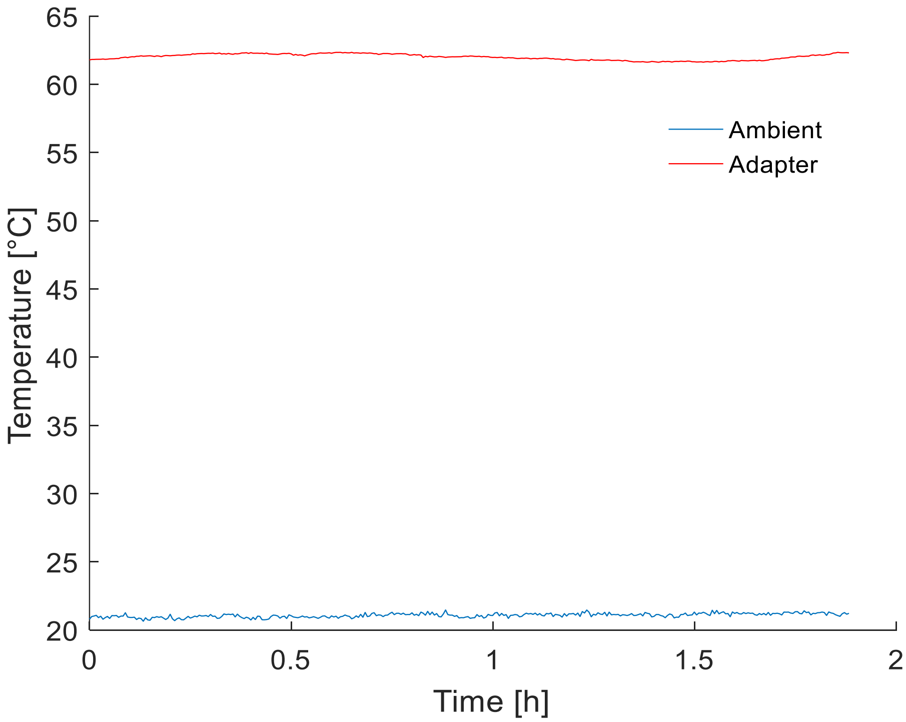

Figure 27. Experiment temperatures for 20, 46.6, 100, 150, and 200 Ω resistors at 100% load (full railcar) and a simulated train speed of 97 km/h

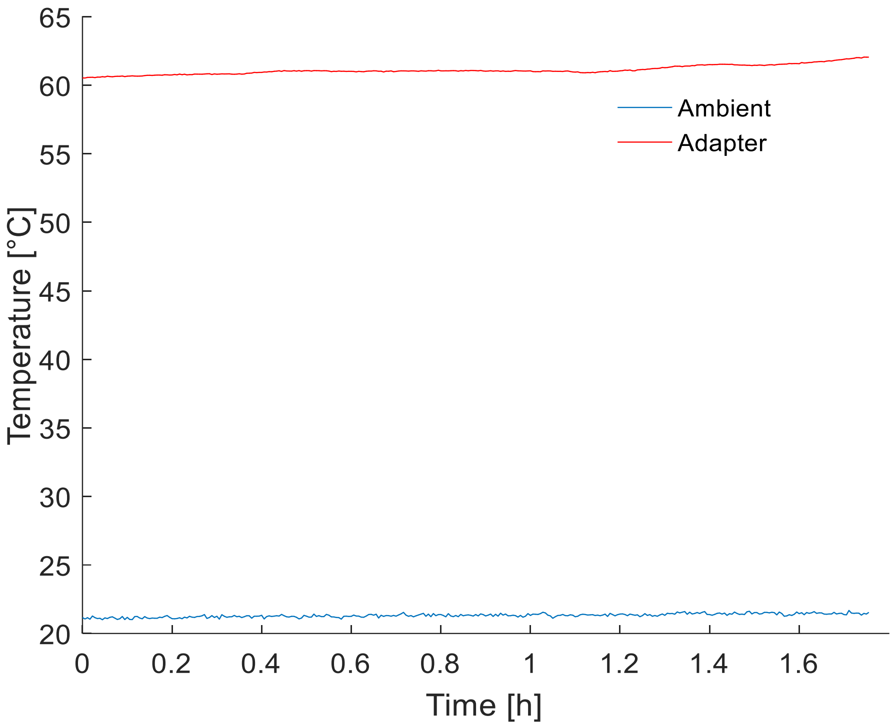

Figure 28. Experiment temperatures for 2, 5, 7, 10, and 15 Ω resistors at 100% load (full railcar) and a simulated train speed of 97 km/h

From the data plotted in Figure 27, the ambient temperature averaged 21°C while the bearing adapter operating temperature increased to an average of about 62°C, producing a temperature difference of 41°C. Similarly, the data from Figure 28 shows the ambient temperature to remain at 21°C while the bearing adapter temperature average about 61°C, generating a temperature difference of 40°C. The resultant voltages at the operating condition of 100% railcar load and a train speed of 97 km/h are presented in Figure 29 and Figure 30, respectively, for the two sets of resistors tested.

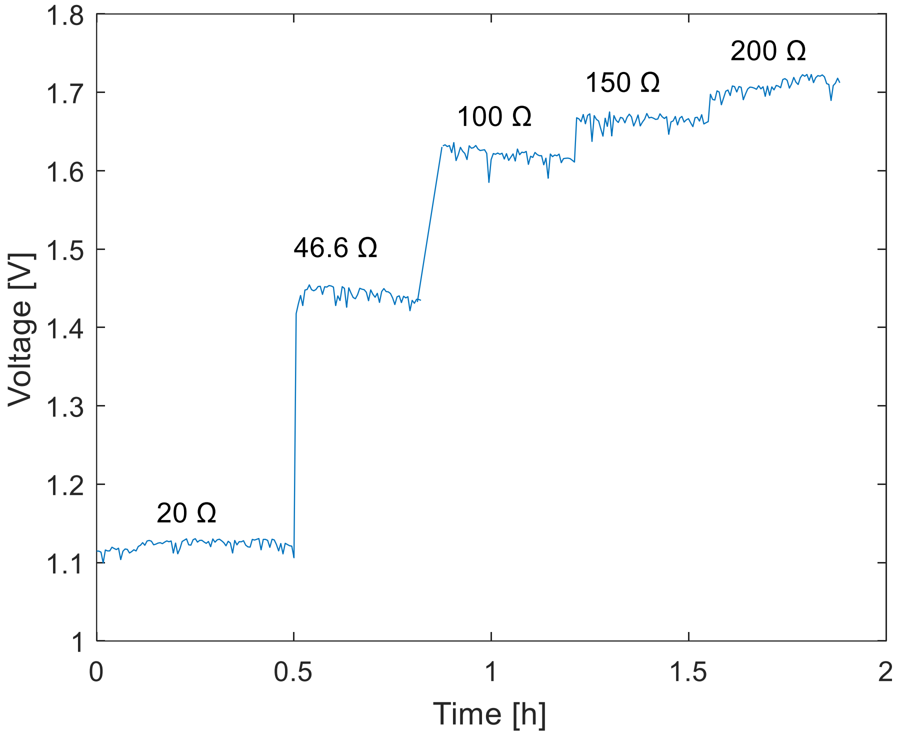

Figure 29. Voltages produced at 100% load (full railcar) across 20,46.6,100,150, and 200 Ω resistors and a simulated train speed of 97 km/h

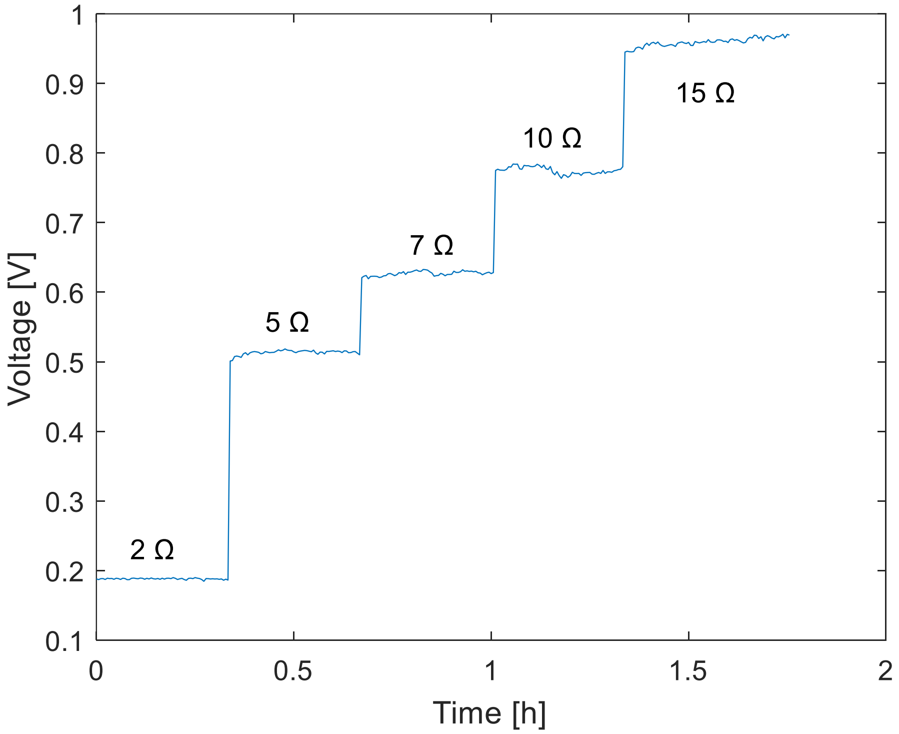

Figure 30. Voltages produced at 100% load (full railcar) across 2,5,7,10, and 15 Ω resistors and a simulated train speed of 97km/h

Table 6 was generated using the data presented in Figure 29 and Figure 30. From this data, it was concluded that a resistance of 15 Ω produced the minimal voltage required to start the boost converter. The highest voltage value of 1.71 V was generated with the 200 Ω resistor, while the highest power of 62.7 mW was produced using the 20 Ω resistor. The data from Table 5 and Table 6 were used to derive the TEG performance plots shown in Figure 31 and Figure 32.

Table 6. Average values for voltage, current, and power produced by the energy harvesters at the different resistor values while operating at 100% load (full railcar) and a simulated train speed of 97 km/h

Resistance [Ω]	**Average Voltage [V]**	**Average Current [mA]**	**Average Power [mW]**
2	0.19	94.0	17.7
5	0.51	102.6	52.6
7	0.63	89.6	56.2
10	0.78	77.5	60.1
15	0.96	63.9	61.3
20	1.12	56.0	62.7
46.6	1.46	31.1	45.1
100	1.62	16.2	26.3
150	1.66	11.1	18.5
200	1.71	8.5	14.6

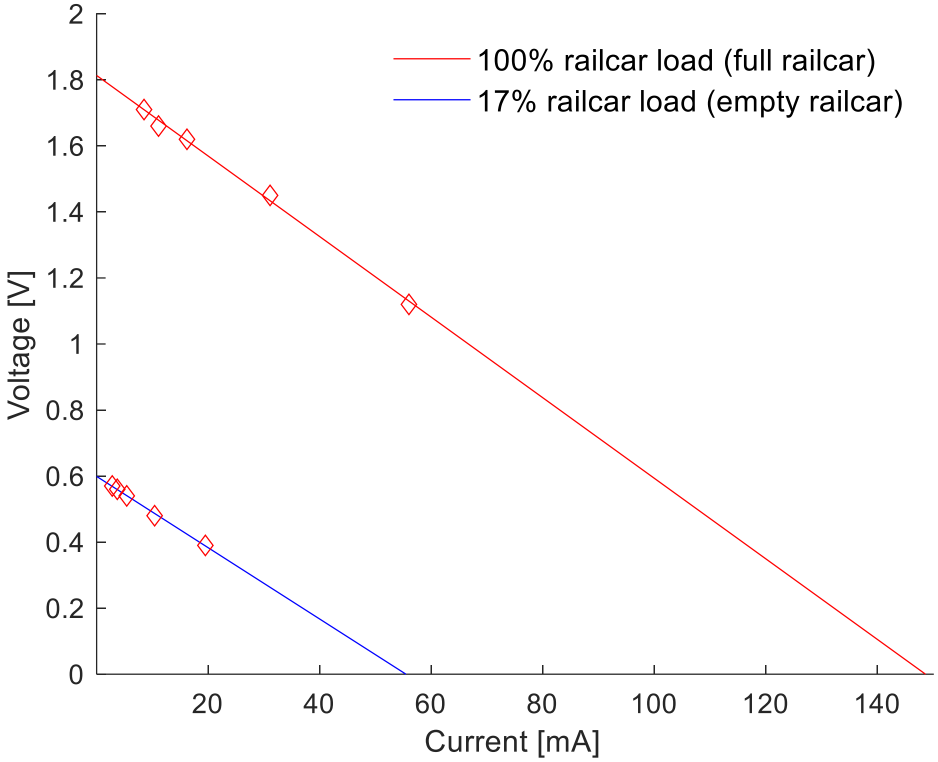

Figure 31. 40×40 mm TEG performance across 20, 46.6, 100, 150, and 200 Ω resistors at 17% and 100% railcar load and a simulated train speed of 97 km/h

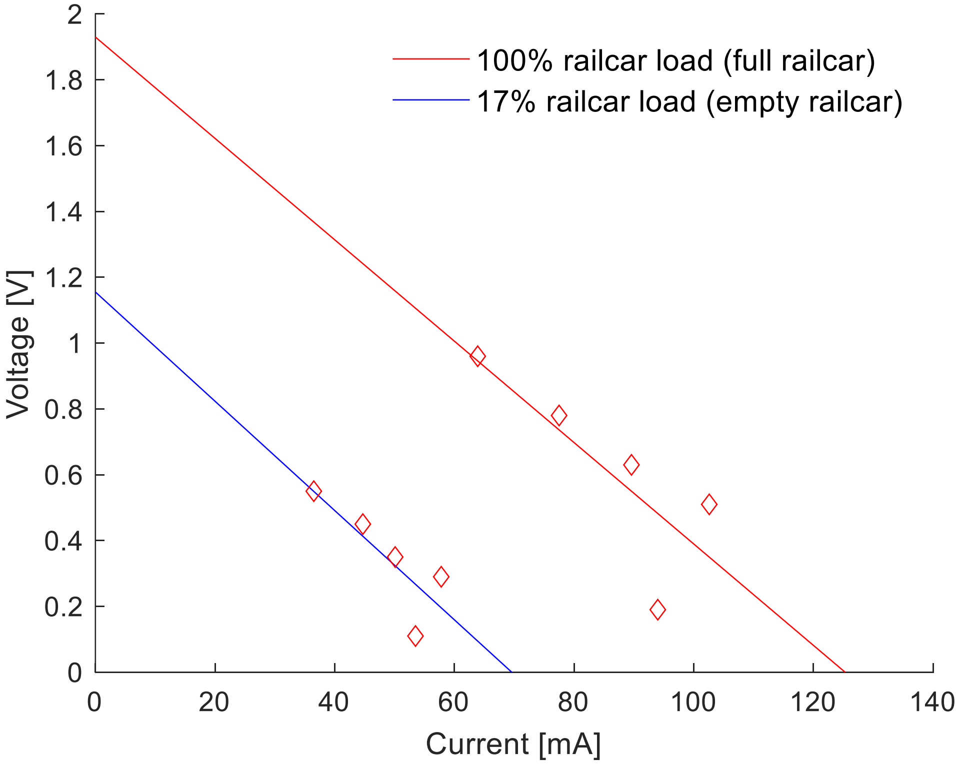

Figure 32. 40×40 mm TEG performance across 2, 5, 7, 10, and 15 Ω resistors at 17% and 100% railcar load and a simulated train speed of 97 km/h

The voltage and current data points from Table 5 and Table 6 were plotted to create the linear trends that will determine the open circuit voltage (V_{oc}) and short circuit current (I_{sc}). Figure 31 presents the data acquired at 17% and 100% railcar load and a simulated train speed of 97 km/h using resistor values of 20, 40.6, 100, 150 and 200 Ω, whereas Figure 32 presents the results for the resistor values of 2, 5, 7, 10, and 15 Ω at the same operating conditions. As mentioned earlier, this data was plotted on two separate graphs since the experiment was repeated for the two different sets of resistors.

At 17% railcar load (i.e., empty railcar load), the V_{oc} and I_{sc} values derived from the higher resistance set (Figure 31) were 0.6 V and 55.47 mA, respectively. This yielded an optimal power value of 8.3 mW at an optimal resistance of 10.8 Ω. The lower resistance set yielded a V_{oc} of 1.16 V and an I_{sc} of 69.59 mA. These values resulted in an optimal power of 20.2 mW at an optimal resistance of 16.7 Ω. The discrepancy between the two sets of resistors tested may be attributed to the surface contact between the adapter and the bearing, and the heat generated within the bearing, which are less consistent at lower railcar loads.

At 100% railcar load (i.e., fully loaded railcar), the V_{oc} obtained with the higher resistance set was at 1.81 V while the I_{sc} was 148.6 mA. This resulted in an optimal power production of 67.2 mW at a resistance of 12.2 Ω. Meanwhile, the lower resistance set yielded a V_{oc} of 1.93 V with an I_{sc} of 125.3 mA resulting in an optimal power generation of 60.5 mW at 15.4 Ω. At full railcar load, both resistance sets yielded similar results indicating that the performance of the TEGs is more consistent under this loading condition.

4.1.2 Experiment 227C (30×30 mm harvesters on bearing adapter)

Experiment 227C utilized two TEG1-1263-4.3 modules wired in series on a four-bearing tester (4BT) adapter. The motor was set to a speed of 796 RPM which correlates to a simulated train traveling speed of 137 km/h (85 mph). Contrary to experiment 228B, this experiment was only conducted at 100% railcar load. The absence of data for the 17% railcar load scenario is later explained in the results. This speed/load combination is representative of a best-case scenario for the 30×30 mm TEGs as these parameters produce ideal conditions for enhanced heat generation within the bearings. The resultant temperature and voltage data under the latter operating conditions for resistor values of 20, 46.6, 100, 150, and 200 Ω are displayed in Figure 33 and Figure 34, respectively. At these operating conditions, the adapter temperature settled at 57°C while the ambient stayed relatively constant at 22°C, resulting in a temperature difference of 35°C.

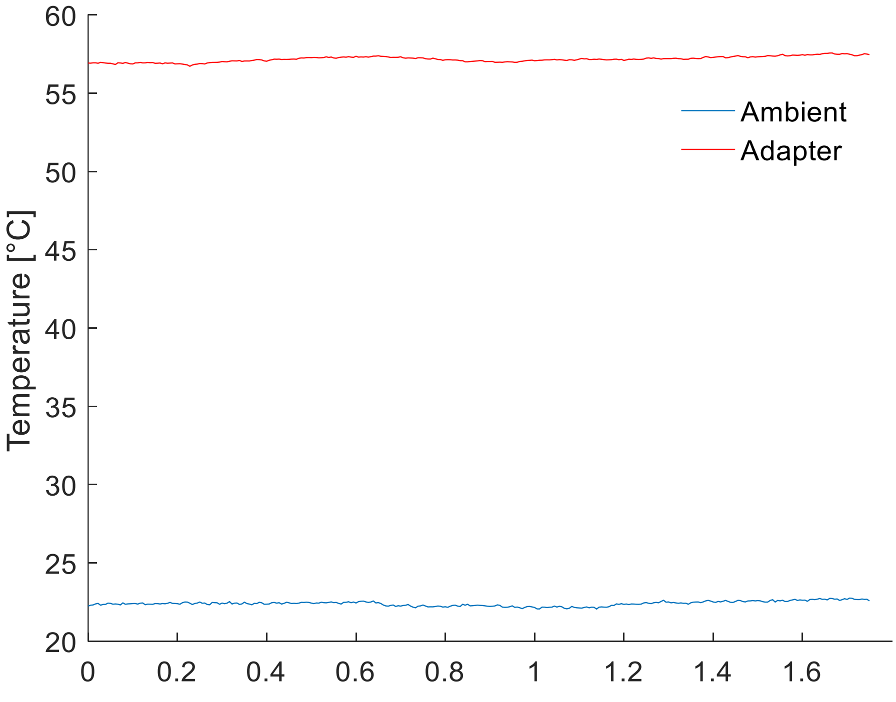

Figure 33. Experiment temperatures for 20, 46.6, 100, 150, and 200 Ω at 100% railcar load (full railcar) and a simulated train speed of 137 km/h

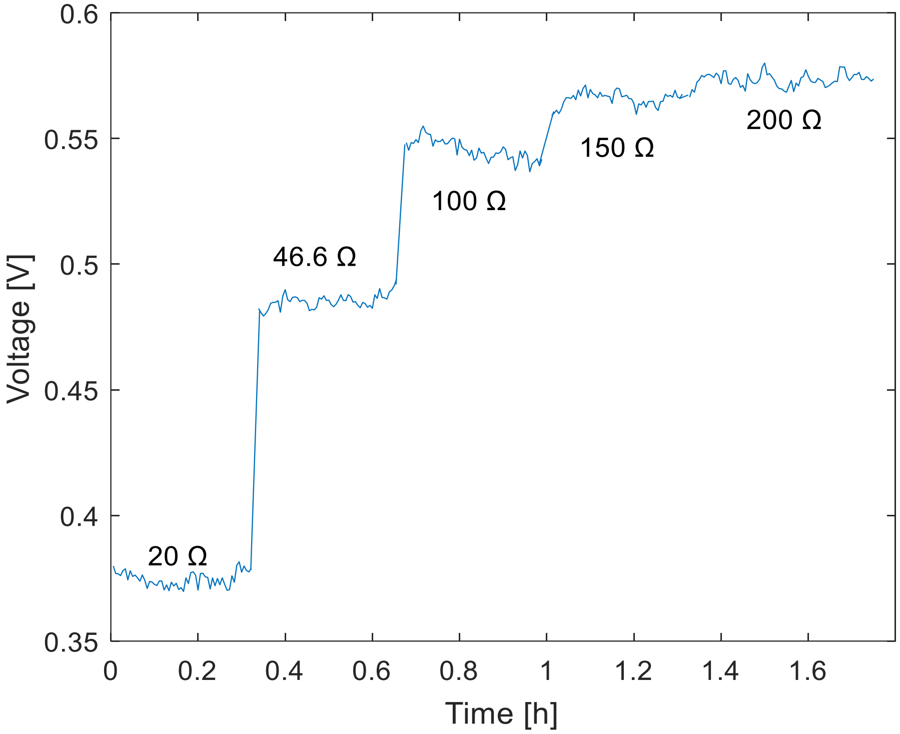

Figure 34. Voltages produced at 100% railcar load across 20, 46.6, 100, 150, and 200 Ω resistors and a simulated train speed of 137 km/h

Table 7 was generated by calculating the average voltage for each resistor shown in Figure 34. These ideal operating conditions produced the highest voltage of 0.57 V at a resistance of 200 Ω, while the highest power generated was 7.0 mW at a 20 Ω resistance.

Table 7. Average values for voltage, current, and power at 100% load (full railcar) and a simulated train speed of 137km/h

Resistance [Ω]	**Average Voltage [V]**	**Average Current [mA]**	**Average Power [mW]**
20	0.38	18.75	7.03
46.6	0.49	10.41	5.05
100	0.55	5.45	2.97
150	0.57	3.77	2.14
200	0.57	2.87	1.64

Figure 35 shows an open circuit voltage of 0.61 V and a short circuit current of 48.61 mA. This yields optimal power and resistance values of 7.4 mW and 12.5 Ω, respectively. Even though these conditions represent a best-case scenario, the 30×30 mm TEGs did not produce enough voltage to start the boost converter in this application, hence, this negated the need to perform testing at the less than favorable 17% railcar load operating conditions. For the same reason, the lower resistances were not tested since the output voltages would be even lower. To produce a sufficient voltage using this model of TEG, either a much higher temperature gradient will have to be introduced (which is not feasible for this application) of more TEGs, wired in series, will have to be mounted on the bearing adapter.

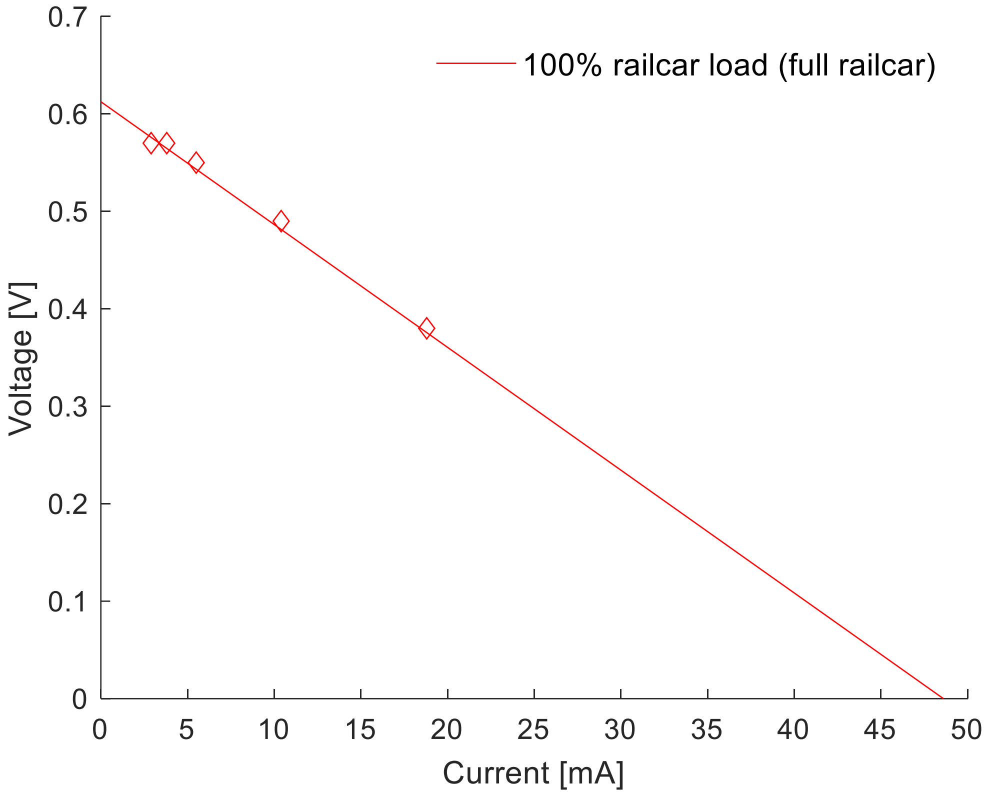

Figure 35. 30×30 mm TEG performance across 20, 46.6, 100, 150, and 200 Ω resistors at 100% load (full railcar) and a simulated train speed of 137 km/h

4.2 Initial Route Testing

The three experiments in this section were performed using the four-bearing chamber tester (4BCT) set at an ambient temperature of 22°C (71.6°F). The tester was fitted with four class F bearings, consisting of three control (defect-free) bearings and one defective bearing containing a cone (inner ring) spall. The defective bearing along with one of the three controls were placed in the middle two positions of the test axle configuration. This replicates field service conditions as these two bearings are top loaded in this setup, as depicted in Figure 20. The tester was equipped with two energy harvesting devices mounted on the middle two bearing adapters to compare the energy harvesting performance of the healthy (control) bearing versus that of the defective bearing. The fans were placed perpendicular to the test rig and supplied a uniform airflow of 6 $\frac{m}{s}$ (13.4 mph). These experiments were carried out executing the test plan for Route 1 described in Table 3.

The objective of the first experiment, in this series of three experiments, was to quantify the amount of charge the energy harvesting device can generate in a round trip. This was achieved by connecting the energy harvesting device to the lithium-ion battery with a coulomb counter between both components to keep track of the charge. The second experiment in the series was conducted to determine the power consumption of the wireless condition monitoring device as it acquired vibration data using a one-second algorithm. For this experiment, the wireless monitoring device was connected to the battery with a coulomb counter in between; and no energy harvesting device was used. Finally, the purpose of the third experiment in this series was to evaluate if the energy harvesting device produced more charge than what was consumed by the wireless monitoring device. In this experiment, the energy harvesting device was connected to the battery and the wireless monitoring module with a coulomb counter placed between the Battery Management Chip (BMC) and the battery.

4.2.1 Energy Harvesting Charging

As explained earlier, the purpose of this experiment was to quantify the amount of charge the energy harvesting device can generate in a single round trip. The lithium-ion batteries used in this experiment were completely drained (0 mAh-milliamp hour) to determine if the energy harvesting device could produce enough current to kickstart the charging process. This is an important criterion since the boost converters require a higher input voltage to self-start than to continue harvesting once initialized. This test was used to assess if a completely discharged battery can recover operation solely from the power generated by the energy harvesting device. The block diagram of Figure 36 shows the wiring of the components used during this experiment. Table 8 through Table 11 give the time, simulated train speed, average ambient temperature (T_{amb}), average bearing adapter temperature (T_{adp}), temperature difference between the bearing adapter and the ambient (ΔT), charge generated, and the average power produced per segment.

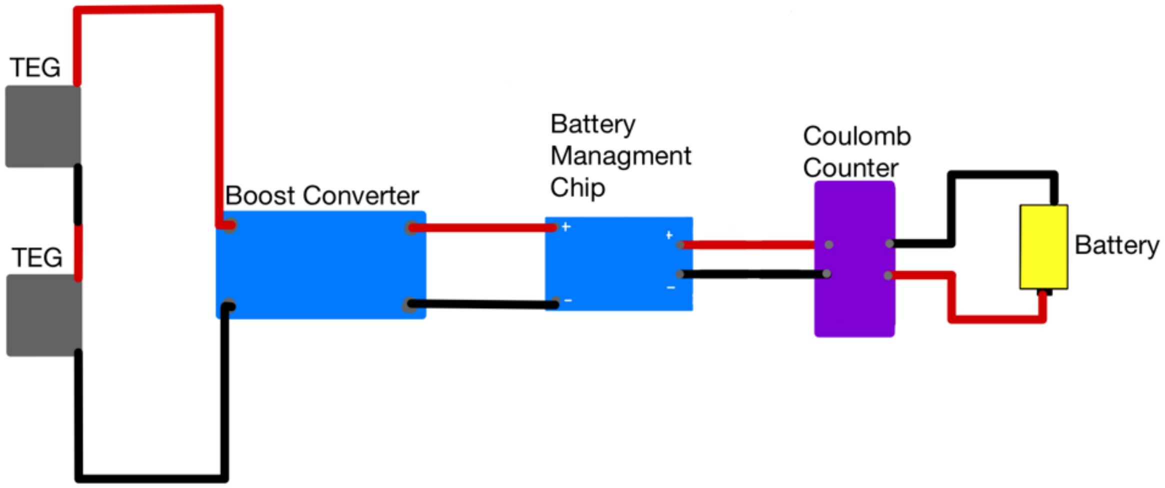

Figure 36. Block diagram for energy harvesting device in a charging scenario

Table 8. Energy harvesting device recharging battery at 100% railcar load – healthy bearing

Time [h]	Speed [rpm]/[mph]	Avg. T_{amb} [°C]	Avg. T_{adp} [°C]	ΔT [°C]	Voltage [V]	Charge [mAh]	Avg. Power [mW]
0.97	234 / 25	21	41	20	3.26	4.27	14.3
0.30	327 / 35	21	43	22	3.27	1.70	18.6
9.83	560 / 60	22	59	37	3.46	128.69	45.3
0.25	498 / 53	22	56	34	3.46	3.08	42.6
0.40	420 / 45	22	54	32	3.47	4.26	37.0
4.01	560 / 60	23	57	34	3.50	48.14	42.0
					Total:	**190.14**	

Table 9. Energy harvesting device recharging battery at 100% railcar load – defective (cone spall) bearing

Time [h]	**Speed [rpm]/[mph]**	**Avg. T_{amb} [°C]**	**Avg. T_{adp} [°C]**	**ΔT [°C]**	**Voltage [V]**	**Charge [mAh]**	**Avg. Power [mW]**
0.97	234 / 25	21	31	10	3.20	0.00	0.0
0.30	327 / 35	21	32	11	3.20	0.00	0.0
9.83	560 / 60	22	53	31	3.41	97.67	33.9
0.25	498 / 53	22	57	35	3.41	2.86	39.0
0.40	420 / 45	22	54	32	3.41	4.10	35.0
4.01	560 / 60	23	57	34	3.44	47.00	40.3
					Total:	**151.63**	

Table 8 and Table 9 show the data collected for both bearings at full railcar load. This portion of the experiment was used to simulate a train traveling to its destination fully loaded. At the initial speeds of the experiment, the temperature difference (ΔT) in the healthy bearing was around 10°C higher than the defective bearing. This resulted in the harvesting device affixed to the healthy bearing generating 14.3 and 18.6 mW of power at speeds of 40 km/h (25 mph) and 56 km/h (35 mph), respectively. In contrast, the energy harvesting device on the defective bearing did not generate any power at those same speeds. The zero-power production is most likely the result of the temperature difference being too low to produce a voltage sufficient to start the boost converter. Once the tester speed was set to 97 km/h (60 mph), the temperature difference between the ambient and the bearing adapter increased significantly. This increase is due to the bearings generating more frictional heating at higher speeds, resulting in the highest power production seen throughout the experiment. At the first half of this experiment, the harvesting device on the healthy bearing produced a total charge of 190.14 mAh or 17.3% of battery charge. In contrast the harvesting device on the defective bearing produced 151.63 mAh or 13.8% of battery charge.

Table 10. Energy harvesting device recharging battery at 17% railcar load – healthy bearing

Time [h]	Speed [rpm]/[mph]	Avg. T_{amb} [°C]	Avg. T_{adp} [°C]	ΔT [°C]	Voltage [V]	Charge [mAh]	Avg. Power [mW]
4.01	560 / 60	21	36	15	3.51	4.79	4.2
0.40	420 / 45	21	36	15	3.51	0.68	6.2
0.25	498 / 53	21	36	15	3.51	0.34	4.8
9.83	560 / 60	22	37	15	3.53	16.72	6.0
0.30	327 / 35	21	36	15	3.53	0.51	6.0
0.97	234 / 25	21	32	11	3.53	0.34	1.2
					Total:	**23.38**	

Table 11. Energy harvesting device recharging battery at 17% railcar load – defective (cone spall) bearing

Time [h]	Speed [rpm]/[mph]	Avg. T_{amb} [°C]	Avg. T_{adp} [°C]	ΔT [°C]	Voltage [V]	Charge [mAh]	Avg. Power [mW]
4.01	560 / 60	21	37	16	3.46	7.51	6.5
0.40	420 / 45	21	38	17	3.46	0.85	7.7
0.25	498 / 53	21	37	16	3.46	0.35	4.8
9.83	560 / 60	22	35	13	3.47	8.70	3.1
0.30	327 / 35	21	32	11	3.47	0.17	2.0
0.97	234 / 25	21	29	8	3.47	0.00	0.0
					Total:	**17.58**	

Once the first half of the experiment concluded, the tester was set to 17% railcar load (simulating an empty railcar load) and ran with a mirrored test plan simulating the train traveling back empty. Table 10 and Table 11 give the results for the two test bearings. The lower railcar load generated less frictional heating within the bearings, which directly impacted the resulting temperature difference between the bearing adapter and the ambient. At the end of the second half of the experiment, the energy harvesting device on the healthy bearing generated up to 23.38 mAh corresponding to 2.1% of battery charge, whereas the device on the defective bearing produced a total of 17.58 mAh which corresponds to 1.6% of battery charge. When considering the roundtrip numbers, the energy harvesting device on the healthy bearing generated a total of 213.52 mAh (i.e., 19.4% of battery charge) while the device on the defective bearing produced a total of 169.21 mAh (i.e., 15.4% of battery charge). Note that the percent battery charge calculations are based on a 100% battery charge of 1100 mAh.

4.2.2 Wireless Onboard Condition Monitoring Device Power Consumption

The second phase of testing was carried out utilizing the same tester/bearing setup with the wireless module being powered by a 14500-battery cells charged to a 100% state of charge (SoC) and no energy harvesting device applied. A block diagram demonstrating the circuitry for this setup is given in Figure 37.

To simulate field service operation, the Lithium-ion battery powered the wireless monitoring device while it was executing the same algorithm designed for field service implementation. The algorithm was programmed to capture one-second of accelerometer data and send it to a receiver unit every 10 minutes. The wireless monitoring module was mounted on a bearing adapter and operated for the same time duration as the previous experiment. However, no change in speeds was necessary since the power draw of the module should stay consistent throughout the experiment as it is independent of both the speed and the bearing operating temperature.

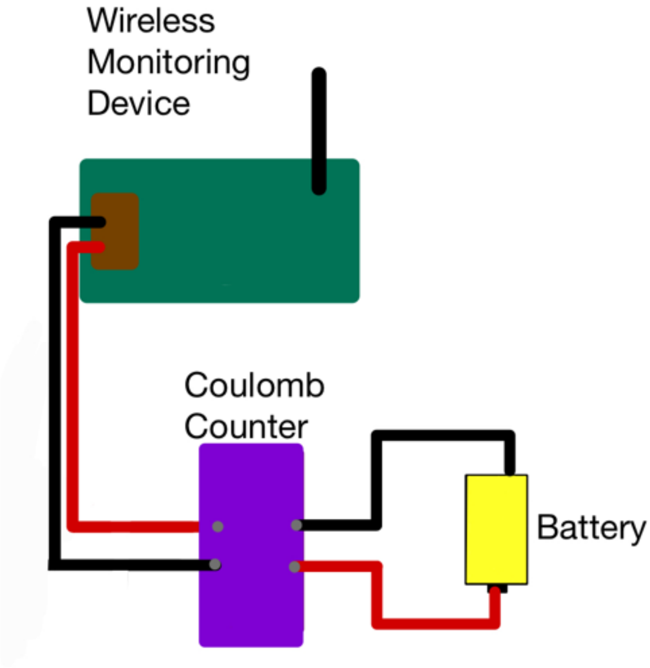

Figure 37. Block diagram for wireless condition monitoring device power consumption test

Table 12. Wireless onboard bearing condition monitoring power consumption

Time [h]	Battery Charge [mAh]	Battery Voltage [V]	Average Current [mA]	Average Power [mW]
0.00	1100.0	4.10	0.0	0.0
1.00	1099.66	4.10	-0.3	-1.4
2.00	1099.15	4.10	-0.5	-2.1
4.00	1098.12	4.10	-0.5	-2.1
6.00	1097.27	4.09	-0.4	-1.7
11.50	1094.37	4.09	-0.5	-2.2
15.76	1092.32	4.09	-0.5	-2.0
24.00	1088.39	4.08	-0.5	-2.0
26.00	1087.54	4.08	-0.4	1.7
28.00	1086.52	4.08	-0.5	-2.1
31.52	1084.81	4.08	-0.5	-2.0
Total Drained:	**-15.19**	**Average:**	**-0.5**	**-1.9**

Table 12 presents the results for the power consumption experiment. The data recorded includes the battery charge, battery voltage, average current, and the average power consumed. The negative values indicate the power consumed rather than generated. For the first half of the trip, the wireless monitoring device consumed 7.68 mAh, while in the second half of the trip, the device consumed 7.51 mAh. Hence, the wireless monitoring device consumed a total of 15.19 mAh or 1.4% of the battery SoC for the roundtrip. In doing so, the wireless monitoring device used an average current and power of 0.5 mA and 1.9 mW, respectfully. With this data, one can deduce that the 1100 mAh (4070 mWh) battery should last up to 2142 hours (three months) of continuous operation in the absence of an energy harvesting device.

4.2.3 Initial Energy Harvesting Performance

For the final phase of testing, the same chamber tester and bearing setup were used with the energy harvesting device now connected to both the battery and the wireless monitoring device as shown in Figure 38. The intent of this test was to establish if the energy harvested was sufficient to keep the wireless monitoring device functional while simultaneously increasing the charge of the battery. The wireless monitoring device utilized the same one-second algorithm to replicate the power draw that would be seen in field service. The 14500 batteries were slightly discharged to around 3.8 Volts to verify if the energy harvested was enough to increase the charge of the batteries.

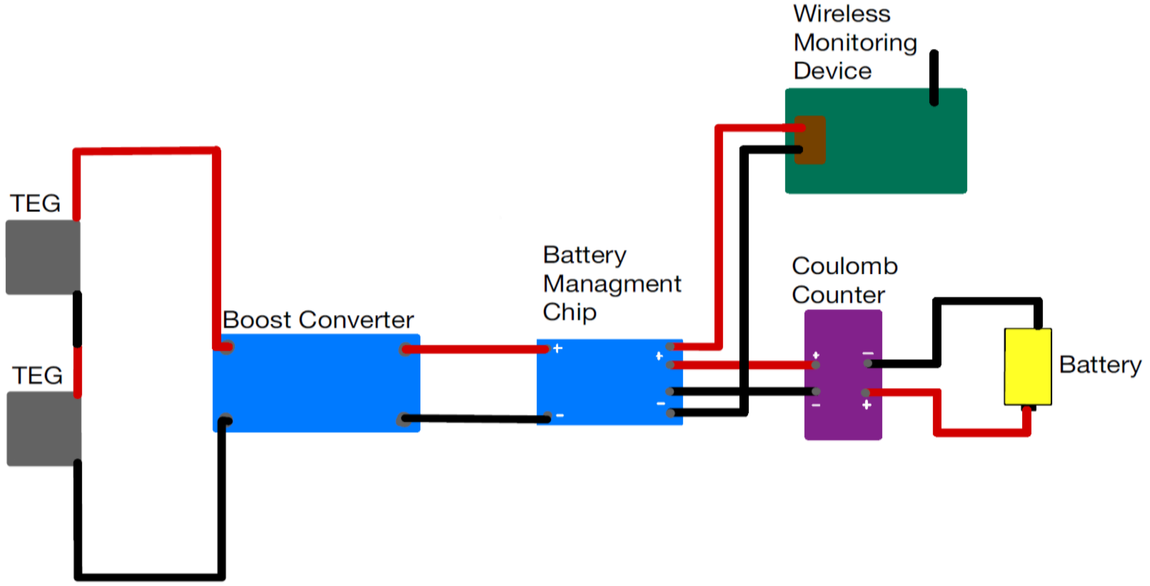

Figure 38. Block diagram of energy harvesting performance experiment setup

Table 13. Overall system performance at 100% railcar load – healthy bearing

Time [h]	**Speed [rpm]/[mph]**	**Avg. T_{amb} [°C]**	**Avg. T_{adp} [°C]**	**ΔT [°C]**	**Voltage [V]**	**Charge [mAh]**	**Avg. Power [mW]**
0.97	234 / 25	22	42	19.8	3.81	2.39	9.4
0.30	327 / 35	22	40	18.1	3.80	0.51	6.5
9.83	560 / 60	23	50	27.5	3.89	65.71	26.0
0.25	498 / 53	23	52	28.7	3.90	2.05	32.0
0.40	420 / 45	23	50	27.3	3.90	2.56	25.0
4.01	560 / 60	23	53	29.8	3.92	36.53	35.7
					Total:	**109.75**	

Table 14. Overall system performance at 100% railcar load – defective (cone spall) bearing

Time [h]	**Speed [rpm]/[mph]**	**Avg. T_{amb} [°C]**	**Avg. T_{adp} [°C]**	**ΔT [°C]**	**Voltage [V]**	**Charge [mAh]**	**Avg. Power [mW]**
0.97	234 / 25	22	35	13	3.82	0.00	0.0
0.30	327 / 35	22	33	11	3.81	0.00	0.0
9.83	560 / 60	23	39	16	3.82	5.98	2.3
0.25	498 / 53	23	40	17	3.83	0.17	2.6
0.40	420 / 45	23	40	17	3.83	0.35	3.4
4.01	560 / 60	23	39	16	3.83	2.90	2.8
					Total:	**9.40**	

Table 13 and Table 14 provide the data collected for the two test bearings at a full railcar load. For the first 1.27 hours of the experiment, the energy harvesting device on the healthy bearing produced 9.4 mW and 6.5 mW for speeds of 40 km/h and 56 km/h (25 mph and 35 mph), respectively. Meanwhile, the energy harvesting device on the defective bearing failed to produce any power. Again, this is attributed to the low temperature difference (ΔT) present between the ambient in the chamber and the bearing adapter. For the first half of the experiment, the energy harvesting device on the healthy bearing generated a total charge of 109.75 mAh (i.e., 10% of battery charge), whereas the energy harvesting on the defective bearing produced a total charge of 9.4 mAh (or 1% of battery charge).

Table 15. Overall system performance at 17% railcar load – healthy bearing

Time [h]	Speed [rpm]/[mph]	Avg. T_{amb} [°C]	Avg. T_{adp} [°C]	ΔT [°C]	Voltage [V]	Charge [mAh]	Avg. Power [mW]
4.01	560 / 60	22	36	14	3.92	-1.71	-1.7
0.40	420 / 45	22	35	13	3.91	-0.17	-1.7
0.25	498 / 53	22	35	13	3.91	-0.17	-2.7
9.83	560 / 60	22	36	14	3.91	-4.09	-1.6
0.30	327 / 35	22	36	14	3.91	-0.18	-2.4
0.97	234 / 25	21	32	11	3.91	-0.51	-2.0
					Total:	**-6.83**	

Table 16. Overall system performance at 17% railcar load – defective (cone spall) bearing

Time [h]	Speed [rpm]/[mph]	Avg. T_{amb} [°C]	Avg. T_{adp} [°C]	ΔT [°C]	Voltage [V]	Charge [mAh]	Avg. Power [mW]
4.01	560 / 60	22	31	9	3.83	-0.85	-0.8
0.40	420 / 45	22	31	9	3.83	-0.17	-1.6
0.25	498 / 53	22	30	8	3.82	-0.17	-2.6
9.83	560 / 60	22	31	9	3.82	-2.39	-0.9
0.30	327 / 35	22	31	9	3.81	-0.17	-2.2
0.97	234 / 25	21	29	8	3.81	-0.52	-2.0
					Total:	**-4.27**	

Table 15 and Table 16 present the data acquired for the two test bearings at an empty railcar load. The data from these sets indicate that the temperature difference (ΔT) during testing was not large enough to produce the necessary voltage to start the boost converter. This resulted in the average power values listed in Table 15 and Table 16 closely resembling the power consumption values in Table 12. During the second half of the experiment, the battery on the healthy bearing lost 6.83 mAh (or 0.6% of battery charge) while the battery in the defective bearing lost 4.27 mAh (or 0.4% of battery charge). Nevertheless, if one considers the roundtrip totals, it appears that the energy harvesting devices on both the healthy and the defective bearing were able to sustain the operation of the wireless onboard condition monitoring modules while also increasing the state of charge (SoC) of the batteries. Moreover, the data suggests that a temperature difference of about 15-20°C must be present between the ambient and the bearing adapter to produce enough power for the boost converter to start charging the battery.

CHAPTER V

FIELD IMPLEMENTATION SIMULATION TESTING

5.1 Field Simulation Testing Improvements

To improve upon the results of the preliminary testing discussed in Chapter IV, several changes were implemented to the test methodology. First, a second coulomb counter was added between the wireless condition monitoring device and the battery management chip (BMC). Unlike the previous test setup, this addition allowed one to distinguish between the energy consumed by the wireless monitoring device and the energy supplied to the battery. Second, multiple routes were tested to compare the amounts of energy that could be harvested between a train traveling in a rural area as opposed to a train traveling in an urban area. Last, the wireless monitoring device algorithm was updated to give the option of executing either the one-second data acquisition program or the four-second data collection program. This modification to the algorithm allowed for the direct comparison of the power consumption when executing the two data acquisition schemes. The main difference between these two algorithm schemes is the amount of data being captured for analysis. Although both algorithm schemes have been proven to accurately and reliably assess the bearing health, the one-second algorithm has been primarily optimized for power consumption, while the four-second algorithm was optimized for enhanced accuracy. The latest version of the wireless condition monitoring device has been improved by adding a filter for noise reduction, a faster central processing unit, and higher RAM memory.

Accordingly, the algorithms were modified to properly function with the hardware revisions. Therefore, quantifying the difference in power consumption between the one-second and four-second data collection schemes allows the user to make sound divisions on how to operate their wireless condition monitoring devices in field service.

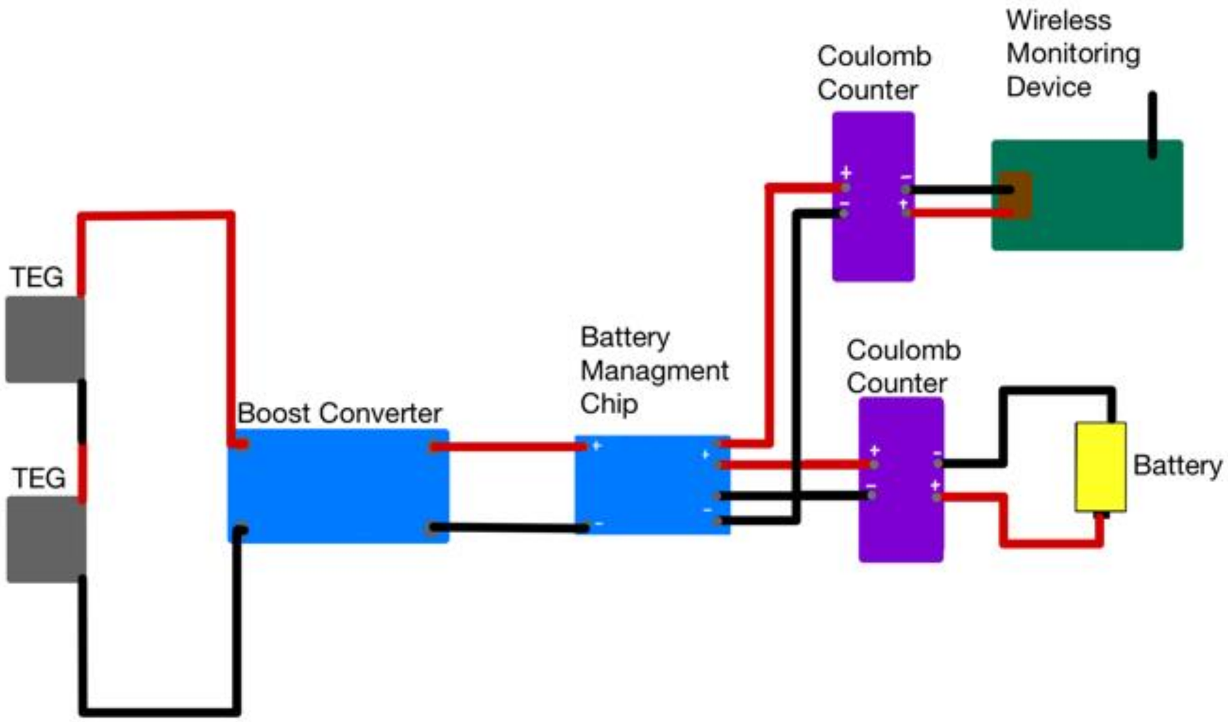

Figure 39 Block diagram for improved route testing setup

All experiments discussed here were conducted on the four-bearing chamber tester (4BCT) with the air conditioning unit set to 21°C (70°F). This was done to help stabilize the ambient temperature of the laboratory since multiple test rigs were being operated at the same time. The 4BCT was fitted with a test axle containing four class K bearings of which three were control (defect-free) bearings and one was a defective bearing containing a cup (outer ring) spall. Like in previous experiments, one of the three control bearings along with the defective bearing were placed in the middle two bearing positions on the test axle. The batteries used were the same 14500 lithium-ion cells which were discharged to 850 mAh or 77% SoC. Table 17 through

Table 28 presents the data acquired from all the experiments performed. Each table includes the segment duration, simulated train speed, average ambient temperature (T_{amb}), average bearing adapter temperature (T_{adp}), temperature difference (ΔT) between T_{adp} and T_{amb}, charge produced, charge consumed, average voltage, average power generated by the harvesting devices, and average power consumed by the wireless monitoring devices.

5.2 Route 2/ One-Second Algorithm/ 10-Minute Interval

This phase of testing utilized the test plan for Route 2 (described in Table 4) to simulate a worst-case scenario trip in which the bearings are not operating at high speeds for long periods of time as they would be in Route 1. The wireless monitoring device used a one-second algorithm that captured one second of data every ten minutes for the entirety of the experiment.

Table 17. Results for Route 2 at 100% railcar load using the one-second algorithm at a 10-minute interval – healthy bearing

Time [h]	**Speed [rpm]/ [mph]**	**Avg. T_{amb} [°C]**	**Avg. T_{adp} [°C]**	**ΔT [°C]**	**Charge Produced [mAh]**	**Charge Consumed [mAh]**	**Voltage [V]**	**Avg. Power Generated [mW]**	**Avg. Power Consumed [mW]**
0.45	234/25	20	33	14	0.00	-0.17	3.84	0.0	-1.5
2.1	327/35	19	36	17	0.00	-1.20	3.84	0.0	-2.2
0.43	514/55	17	39	21	0.34	-0.17	3.85	1.3	-1.5
0.2	420/45	20	43	23	0.34	-0.17	3.85	1.3	-3.3
1.61	560/60	18	48	30	9.05	-1.53	3.87	35.0	-3.7
0.5	514/55	19	50	31	3.07	-0.17	3.87	11.9	-1.3
1	420/45	18	46	28	4.78	-0.86	3.87	18.5	-3.3
2.1	327/35	18	39	20	2.05	-1.19	3.87	7.9	-2.2
2.7	234/25	19	34	15	0.00	-1.54	3.87	0.0	-2.2
				Total:	19.63	-7.00			

Table 18. Results for Route 2 at 100% railcar load using the one-second algorithm at a 10-minute interval – defective (cup spall) bearing

Time [h]	**Speed [rpm]/ [mph]**	**Avg. T_{amb} [°C]**	**Avg. T_{adp} [°C]**	**ΔT [°C]**	**Charge Produced [mAh]**	**Charge Consumed [mAh]**	**Voltage [V]**	**Avg. Power Generated [mW]**	**Avg. Power Consumed [mW]**
0.45	234/25	20	34	15	0.00	-0.17	3.82	0.0	-0.6
2.1	327/35	19	37	18	0.34	-1.20	3.82	1.3	-4.6
0.43	514/55	17	39	21	0.34	-0.34	3.83	1.3	-1.3
0.2	420/45	20	41	21	0.34	-0.17	3.83	1.3	-0.7
1.61	560/60	18	46	28	5.64	-0.85	3.84	21.7	-3.3
0.5	514/55	19	49	31	2.39	-0.17	3.85	9.2	-0.7
1	420/45	18	47	29	3.75	-0.51	3.85	14.4	-2.0
2.1	327/35	18	40	21	2.05	-1.37	3.85	7.9	-5.3
2.7	234/25	19	34	15	0.00	-1.71	3.84	0.0	-6.6
				Total:	14.85	-6.49			

The data in Table 17 and Table 18 display the results for the bearings at full railcar load. At the beginning of the experiment, the temperature difference (ΔT) was similar in both bearings, albeit the defective bearing was able to produce 1.3 mW of power at 35 mph while the healthy bearing produced 0 mW. Although the defective bearing had a 1°C higher temperature difference, this difference is insignificant and both harvesting devices should have produced the same amount of power. It is theorized that although the TEGs on both bearings were producing roughly the same amount of voltage, the boost converters connected to the harvesting devices might have different tolerances in the voltage needed for the boost converter to initialize. Results showed the healthy bearing producing a total charge of 19.63 mAh, whereas the defective bearing produced 14.85 mAh. Meanwhile, the wireless monitoring device consumed 7.00 mAh for the healthy bearing and 6.49 mAh for the defective bearing. Although Route 2 is 4.5 hours shorter than Route 1, it was determined that the combination of the modifications to the wireless monitoring device hardware along with the revisions to the algorithm resulted in a slightly higher power consumption than in previous iterations.

Table 19. Results for Route 2 at 17% railcar load using the one-second algorithm at a 10-minute interval – healthy bearing

Time [h]	**Speed [rpm]/ [mph]**	**Avg. T_{amb} [°C]**	**Avg. T_{adp} [°C]**	**ΔT [°C]**	**Charge Produced [mAh]**	**Charge Consumed [mAh]**	**Voltage [V]**	**Avg. Power Generated [mW]**	**Avg. Power Consumed [mW]**
2.7	234/25	19	26	7	0.00	-1.37	3.86	0.0	-5.3
2.1	327/35	19	27	9	0.00	-1.19	3.86	0.0	-4.6
1	420/45	19	29	10	0.00	-0.51	3.86	0.0	-2.0
0.5	514/55	18	31	13	0.00	-0.34	3.86	0.0	-1.3
1.61	560/60	18	34	15	0.00	-0.86	3.86	0.0	-3.3
0.2	420/45	19	35	16	0.00	-0.17	3.86	0.0	-0.7
0.43	514/55	18	34	16	0.00	-0.17	3.86	0.0	-0.7
2.1	327/35	19	31	13	0.00	-1.19	3.86	0.0	-4.6
0.45	234/25	18	29	11	0.00	-0.34	3.86	0.0	-1.3
				Total:	0.00	-6.14			

Table 20. Results for Route 2 at 17% railcar load using the one-second algorithm at a 10-minute interval – defective (cup spall) bearing

Time [h]	**Speed [rpm]/ [mph]**	**Avg. T_{amb} [°C]**	**Avg. T_{adp} [°C]**	**ΔT [°C]**	**Charge Produced [mAh]**	**Charge Consumed [mAh]**	**Voltage [V]**	**Avg. Power Generated [mW]**	**Avg. Power Consumed [mW]**
2.7	234/25	19	25	6	0.00	-1.54	3.84	0.0	-5.9
2.1	327/35	19	26	7	0.00	-1.19	3.83	0.0	-4.6
1	420/45	19	28	9	0.00	-0.51	3.83	0.0	-2.0
0.5	514/55	18	29	11	0.00	-0.34	3.83	0.0	-1.3
1.61	560/60	18	31	13	0.00	-0.86	3.83	0.0	-3.3
0.2	420/45	19	32	13	0.00	-0.17	3.83	0.0	-0.7
0.43	514/55	18	32	13	0.00	-0.17	3.83	0.0	-0.7
2.1	327/35	19	29	11	0.00	-1.36	3.83	0.0	-5.2
0.45	234/25	18	28	9	0.00	-0.18	3.84	0.0	-0.7
				Total:	0.00	-6.32			

Table 19 and Table 20 summarize the results for both test bearings at an empty railcar load. The results show that the temperature difference (ΔT) for both bearings was too low to initiate the boost converter, which resulted in the batteries to have a lower charge at the end of the empty railcar segment as no charge was added to the batteries. The wireless monitoring devices on the healthy and defective bearing consumed approximately equal amounts of charge, i.e., 6.14 mAh and 6.32 mAh, respectively. Regardless, when the total charge produced and consumed for the loaded (100%) and unloaded (17%) trip segments are summed to simulate a complete roundtrip, both batteries ended with a higher charge, albeit very small increment, than what they had at the beginning of the roundtrip. In more detail, the harvesting device on the healthy bearing increased the battery charge by 6.49 mAh (or 0.6%, of SoC), whereas the harvesting device on the defective bearing increased the battery charge by 2.04 mAh or 0.2% of SoC).

5.3 Route 1/ Four-Second Algorithm/ 10-Minute Interval

This experiment was conducted using the test plan for route 1. This route passed through a rural area which implies that the test rig was used to simulate a train traveling at high speeds for long periods of time. This route represents a best-case scenario for this application since the heat generated within the bearings increases with operating speed which leads to larger temperature differences between the ambient and the bearing adapter temperature and thus, more energy harvesting potential. The wireless monitoring device utilized the four-second algorithm which captured and transmitted four seconds of data every 10-minutes.

Table 21. Results for Route 1 at 100% railcar load using the four-second algorithm at a 10-minute interval – healthy bearing

Time [h]	Speed [rpm]/ [mph]	Avg. T_{amb} [°C]	Avg. T_{adp} [°C]	ΔT [°C]	Charge Produced [mAh]	Charge Consumed [mAh]	Voltage [V]	Avg. Power Generated [mW]	Avg. Power Consumed [mW]
0.97	234/25	18	36	18	0.17	-0.51	3.84	0.7	-2.0
0.3	327/35	19	37	19	0.17	-0.17	3.87	2.2	-2.2
9.83	560/60	18	50	32	64.86	-6.83	3.92	25.9	-2.7
0.25	498/53	17	50	33	1.71	-0.17	3.94	26.9	-2.7
0.4	420/45	18	48	30	2.21	-0.35	3.94	21.8	-3.4
4.01	560/60	18	48	30	21.85	-1.48	3.94	21.5	-1.5
Total:					90.97	-9.51			

Table 22. Results for Route 1 at 100% railcar load using the four-second algorithm at a 10-minute interval – defective (cup spall) bearing

Time [h]	Speed [rpm]/ [mph]	Avg. T_{amb} [°C]	Avg. T_{adp} [°C]	ΔT [°C]	Charge Produced [mAh]	Charge Consumed [mAh]	Voltage [V]	Avg. Power Generated [mW]	Avg. Power Consumed [mW]
0.97	234/25	18	35	17	0.51	-0.51	3.84	2.0	-2.0
0.3	327/35	19	36	17	0.17	-0.17	3.87	2.2	-2.2
9.83	560/60	18	49	32	63.49	-5.81	3.91	25.3	-2.3
0.25	498/53	17	49	32	1.71	-0.19	3.93	26.9	-3.0
0.4	420/45	18	47	29	1.88	-0.15	3.93	18.5	-1.5
4.01	560/60	18	49	31	23.04	-1.88	3.94	22.6	-1.8
Total:					90.80	-8.71			

Table 21 and Table 22 provide the results for both test bearings at full railcar load. In this dataset, the temperature difference (Δ*T*) for both test bearings (healthy and defective) were similar. At the initial speeds of 40 and 56 km/h (25 and 35 mph), both test bearings had temperature difference values ranging from 17°C to 19°C, which resulted in a power generation of up to 2.2 mW at 56 km/h. Once the tester speed was raised to 97 km/h (60 mph), the temperature difference for both test bearings increased markedly to around 33°C. At these high operating speeds, the amount of power generated by the energy harvesters increased significantly. Both test bearings were able to generate a maximum of 26.9 mW after an extended operation at 97 km/h. At the conclusion of this experiment, the results showed that both the healthy and the defective bearing generated around 91 mAh (or 8% SoC) while the wireless monitoring devices on both test bearings consumed about 9 mAh (~1% SoC).

Table 23. Results for Route 1 at 17% railcar load using the four-second algorithm at a 10-minute interval – healthy bearing

Time [h]	Speed [rpm]/ [mph]	Avg. T_{amb} [°C]	Avg. T_{adp} [°C]	ΔT [°C]	Charge Produced [mAh]	Charge Consumed [mAh]	Voltage [V]	Avg. Power Generated [mW]	Avg. Power Consumed [mW]
4.01	560/60	18	34	17	0.00	-2.39	3.94	0.0	-2.3
0.4	420/45	18	37	19	0.85	-0.17	3.94	8.4	-1.7
0.25	498/53	19	36	17	0.17	-0.17	3.94	2.7	-2.7
9.83	560/60	20	36	17	0.00	-5.80	3.94	0.0	-2.3
0.3	327/35	20	35	16	0.00	-0.17	3.94	0.0	-2.2
0.97	234/25	20	32	12	0.00	-0.52	3.93	0.0	-2.1
Total:					1.02	-9.22			

Table 24. Results for Route 1 at 17% railcar load using the four-second algorithm at a 10-minute interval – defective (cup spall) bearing

Time [h]	Speed [rpm]/ [mph]	Avg. T_{amb} [°C]	Avg. T_{adp} [°C]	ΔT [°C]	Charge Produced [mAh]	Charge Consumed [mAh]	Voltage [V]	Avg. Power Generated [mW]	Avg. Power Consumed [mW]
4.01	560/60	18	30	12	0.17	-2.39	3.93	0.2	-2.3
0.4	420/45	18	32	14	0.17	-0.17	3.93	1.7	-1.7
0.25	498/53	19	32	13	0.00	-0.17	3.93	0.0	-2.7
9.83	560/60	20	33	14	0.00	-5.97	3.93	0.0	-2.4
0.3	327/35	20	32	13	0.00	-0.18	3.93	0.0	-2.4
0.97	234/25	20	30	10	0.00	-0.68	3.92	0.0	-2.7
Total:					0.34	-9.56			

Table 23 and Table 24 present the results for the experiment at an empty railcar load. The results exhibit a noticeably lower temperature difference (ΔT) between the bearing adapter and the ambient across all trip segments, for both test bearings, when compared to the data for full railcar load. This directly impacted the amount of charge added to the batteries which, as the data demonstrates, did not exceed 1 mAh. The charge produced was marginal compared to the charge consumed by the wireless monitoring devices which was roughly nine times more. This led to the batteries losing charge during the return segment of the tip due to the low temperature difference. Nevertheless, enough charge was generated during the outgoing segment of the tip to offset the losses during the return segment. When summing the total charge produced and consumed for the complete roundtrip, the energy harvesters on both test bearings generated about 73 mAh, thus increasing the state of charge (SoC) of the batteries by roughly 7% while simultaneously powering the wireless monitoring devices that were executing the four-second algorithm at 10-minute intervals.

5.4 Route 2/ Four-second algorithm/ 10-minute interval

The purpose of the final experiment performed was to verify the performance of the energy harvesters at unfavorable conditions to simulate a worst-case scenario for this application. To that end, Route 2 was used with the wireless monitoring devices executing the four-second algorithm every 10 minutes. This test aimed to determine if the temperature difference (ΔT) generated at unfavorable operating conditions was sufficient to produce more power than what was consumed.

Table 25. Results for Route 2 at 100% railcar load using the four-second algorithm at a 10-minute interval – healthy bearing

Time [h]	Speed [rpm]/ [mph]	Avg. T_{amb} [°C]	Avg. T_{adp} [°C]	ΔT [°C]	Charge Produced [mAh]	Charge Consumed [mAh]	Voltage [V]	Avg. Power Generated [mW]	Avg. Power Consumed [mW]
0.45	234/25	20	41	21	0.34	-0.17	3.90	2.9	-1.5
2.1	327/35	20	42	22	2.90	-1.37	3.90	5.4	-2.5
0.43	514/55	17	43	26	1.37	-0.34	3.90	12.4	-3.1
0.2	420/45	17	45	28	0.85	-0.17	3.91	16.6	-3.3
1.61	560/60	17	51	34	10.58	-1.70	3.92	25.8	-4.1
0.5	514/55	17	52	35	3.93	-0.17	3.93	30.9	-1.3
1	420/45	18	48	30	5.63	-0.70	3.93	22.1	-2.7
2.1	327/35	18	40	22	3.06	-1.37	3.93	5.7	-2.6
2.7	234/25	18	34	16	0.17	-1.54	3.92	0.2	-2.2
				Total:	28.83	-7.53			

Table 26. Results for Route 2 at 100% railcar load using the four-second algorithm at a 10-minute interval – defective (cup spall) bearing

Time [h]	Speed [rpm]/ [mph]	Avg. T_{amb} [°C]	Avg. T_{adp} [°C]	ΔT [°C]	Charge Produced [mAh]	Charge Consumed [mAh]	Voltage [V]	Avg. Power Generated [mW]	Avg. Power Consumed [mW]
0.45	234/25	20	40	20	0.68	-0.17	3.89	5.9	-1.5
2.1	327/35	20	40	20	4.44	-1.20	3.89	8.2	-2.2
0.43	514/55	17	42	24	1.71	-0.34	3.90	15.5	-3.1
0.2	420/45	17	44	27	1.02	-0.17	3.90	19.9	-3.3
1.61	560/60	17	55	38	13.48	-1.72	3.91	32.8	-4.2
0.5	514/55	17	56	39	4.51	-0.17	3.92	35.4	-1.3
1	420/45	18	52	34	6.93	-0.51	3.92	27.2	-2.0
2.1	327/35	18	43	25	5.46	-1.20	3.92	10.2	-2.2
2.7	234/25	18	37	19	1.20	-1.53	3.91	1.7	-2.2
				Total:	39.43	-7.01			

The data in Table 25 and Table 26 summarize the results for both test bearings at full railcar load. On average, the temperature difference (ΔT) was greater for the defective bearing compared to the healthy bearing. This led to the harvesting device on the healthy bearing producing 28.83 mAh while the harvesting device on the defective bearing produced 39.43 mAh. Meanwhile, the power consumed by the wireless monitoring device was similar for both bearings.

Table 27. Results for Route 2 at 17% railcar load using the four-second algorithm at a 10-minute interval – healthy bearing

Time [h]	Speed [rpm]/ [mph]	Avg. T_{amb} [°C]	Avg. T_{adp} [°C]	ΔT [°C]	Charge Produced [mAh]	Charge Consumed [mAh]	Voltage [V]	Avg. Power Generated [mW]	Avg. Power Consumed [mW]
2.7	234/25	19	26	7	0.00	-1.54	3.91	0.0	-2.2
2.1	327/35	20	29	8	0.00	-1.19	3.91	0.0	-2.2
1	420/45	20	31	10	0.00	-0.51	3.91	0.0	-2.0
0.5	514/55	19	32	13	0.00	-0.34	3.91	0.0	-2.7
1.61	560/60	20	37	17	0.00	-0.86	3.91	0.0	-2.1
0.2	420/45	21	39	19	0.17	-0.17	3.91	3.3	-3.3
0.43	514/55	19	39	19	0.34	-0.34	3.91	3.1	-3.1
2.1	327/35	20	35	15	0.17	-1.19	3.91	0.3	-2.2
0.45	234/25	20	32	12	0.00	-0.35	3.91	0.0	-3.0
				Total:	0.68	-6.49			

Table 28. Results for Route 2 at 17% railcar load using the four-second algorithm at a 10-minute interval – defective (cup spall) bearing

Time [h]	Speed [rpm]/ [mph]	Avg. T_{amb} [°C]	Avg. T_{adp} [°C]	ΔT [°C]	Charge Produced [mAh]	Charge Consumed [mAh]	Voltage [V]	Avg. Power Generated [mW]	Avg. Power Consumed [mW]
2.7	234/25	19	27	8	0.00	-1.54	3.91	0.0	-2.2
2.1	327/35	20	29	9	0.00	-1.19	3.91	0.0	-2.2
1	420/45	20	31	11	0.00	-0.68	3.91	0.0	-2.7
0.5	514/55	19	33	13	0.00	-0.17	3.91	0.0	-1.3
1.61	560/60	20	36	17	0.17	-1.03	3.91	0.4	-2.5
0.2	420/45	21	39	18	0.00	-0.17	3.91	0.0	-3.3
0.43	514/55	19	39	20	0.17	-0.17	3.91	1.5	-1.5
2.1	327/35	20	35	15	0.17	-1.37	3.91	0.3	-2.6
0.45	234/25	20	32	12	0.00	-0.17	3.91	0.0	-1.5
				Total:	0.51	-6.49			

Table 27 and Table 28 display the results for both test bearings at an empty railcar load. In this set of data, the temperature difference (ΔT) was too low for the energy harvesting devices to produce more energy than what was consumed by the wireless monitoring device. For both test bearings, the energy harvesting devices produced negligible amounts of charge while the wireless monitoring devices consumed an identical 6.49 mAh of charge. Although the energy harvesting devices were not able to add more charge during the empty railcar portion of the trip, both batteries ended with more charge than what they started with when considering the complete roundtrip. The harvesting device on the healthy bearing was able to add a total charge of 15.5 mAh which corresponds to an increase in the battery SoC of about 1.4%, whereas the harvesting device on the defective bearing was able to add a total charge of 26.5 mAh corresponding to an increase in the battery SoC of about 2.5%.

CHAPTER VI

CONCLUSIONS AND FUTURE WORK

To improve the longevity of a wireless onboard condition monitoring sensor module, an energy harvesting device was developed to prolong its battery life. Various harvesting techniques were analyzed to determine the best method for this application; after which thermoelectricity was selected. With their solid-state design, minimal maintenance, universal mounting capability, and adequate energy output, thermoelectric generators are an ideal element for this prototype device. If implemented correctly, the energy harvesting system should be able to produce enough energy to power the wireless monitoring device as long as the train is in motion. The data acquired from the performed experiments provides a proof-of-concept validation for the complete energy harvesting device which is composed of TEGs, heat sinks, a boost converter, and a battery management chip (BMC).

6.1 Test Results

Using the information gathered from all the conducted experiments, it was concluded that there is a sufficient temperature gradient present in the setup to recharge the 14500 lithium-ion batteries while they simultaneously power a functioning wireless monitoring device. The first phase of testing determined that two TEG2-126LDT (40×40 mm) modules in series hold the ability to generate up to 60 mW of power before taking losses into account. At this rate, the energy harvesting device would be able to fully charge the 1100 mAh (4070 mWh) battery within 67 hours of operation. This is sufficient energy to power low energy components such as the accelerometers and temperature sensors used by the wireless module. Nevertheless, not every TEG model produced adequate results. The TEG1-1263-4.3 (30×30 mm) did not perform to the desired specification because it did not produce enough open-circuit voltage at low temperature differences. Unlike the 40×40 mm TEG, the 30×30 mm TEG is not designed to work at relatively low temperature differences. Instead, the smaller form factor makes it an attractive option to place in tighter locations along the bearing adapter to harvest larger amounts of energy if needed.

An initial test plan was devised to measure different performance metrics of the complete energy harvesting device and the wireless monitoring device. One experiment was used to quantify the amount of energy produced in a roundtrip using a completely drained battery cell. Not only was the energy harvesting device able to produce enough current to initiate the charging sequence of the dead battery, but it also managed to increase the state of charge (SoC) of the battery anywhere from 15% to 20% on a single trip. Further experiments were used to determine the power consumption of the wireless monitoring device. It was found that the wireless monitoring device can consume anywhere from 2-7 mW of energy, depending on the algorithm it executes. It was later found that newer revisions of the wireless monitoring device consumed more energy than what was initially determined. This was due to two main reasons, namely: (1) the newer devices had additional components to provide signal noise reduction and enhanced memory and storage capacity, and (2) the lack of optimization of the communication protocol used to transfer data between the wireless module and the receiver.

Route simulation tests were carried out to validate the performance of the thermoelectric-based energy harvesting device in different use case scenarios. Different routes were used to compare the heat generated within the bearings in a rural and an urban setting. Different algorithm schemes were implemented to determine if the energy harvested during operation was enough to offset the energy consumed by the wireless monitoring device. It was concluded from the testing results that the energy harvesting device was able to increase the charge of the batteries regardless of route or algorithm combination.

6.2 Design Limitations

Although the data in this thesis is adequate to validate the performance of the energy harvesting device with a high level of confidence, there was one limitation that could be eliminated to further improve the results produced in the experiments. The limitation is related to the test rig setup and the available fan speed settings. Even though the fans in the laboratory accurately reproduce an airspeed that closely resembles the wind conditions in field service, the wind produced by the fans cannot dynamically adjust to match the windspeed as the train changes its traveling speed. Nevertheless, this indicates that the results generated in this thesis are conservative estimates of the power produced by the energy harvesting device. This is due to faster wind speeds producing enhanced forced convection which can lead to a higher temperature differential between the sides of the thermoelectric generator and thus more power generation by the energy harvesting device.

6.3 Future Work

Although the data collected from the experiments proved the ability of the harvesting device to increase the charge of the batteries during operation, multiple steps can be taken to further improve the amount of energy that can be harvested. By implementing a pressure mounting system for the TEGs, the use of a thermal adhesive can be eliminated and thus improve heat transfer between the components. This solution will also make it easier to perform maintenance on these devices since adhesive cure time will no longer be an issue. Additionally, smoothing the bearing adapter surface at the locations where the energy harvesting device would be mounted will help improve surface contact between the components, thus reducing thermal contact resistance and enhancing performance. Finally, a future prototype energy harvesting device with a lower self-start voltage will be explored. Although the energy harvesting device works well at full railcar load, implementing a boost converter that has a lower operating voltage would help capture some of the energy harvested at lower temperature differentials as seen in empty railcar load scenarios.

REFRENCES

[1] AAR Railroad 101 Freight Railroads Fact Sheet [Internet] [Accessed 2021 June 2] Available from: https://www.aar.org/wp-content/uploads/2020/08/AAR-Railroad-101-Freight-Railroads-Fact-Sheet.pdf

[2] Economic and Fiscal Impact Analysis of Class I Railroads in 2017 [Internet] [Accessed 2021 June 2] Available from: https://www.aar.org/wp-content/uploads/2018/11/AAR-Class-I-Railroad-Towson-Economic-Impact-October-2018.pdf

[3] AAR Economic Impact Fact Sheet [Internet] [Accessed 2021 June 3] Available from: https://www.aar.org/wp-content/uploads/2020/08/AAR-Economic-Impact-Fact-Sheet.pdf

[4] Federal Railroad Administration Safety Data [Internet] [Accessed 2021 June 5] Available from: https://safetydata.fra.dot.gov/officeofsafety/publicsite/query/inccaus.aspx

[5] Hongru. (n.d.). Retrieved August 11, 2020, from http://www.cccme.org.cn/products/detail-8196521.aspx.

[6] TADS Trackside Acoustic Detection System [Internet] [Accessed 2021 June 5] Available from: https://aar.com/pdfs/TADSupdate_20160615.pdf

[7] Data Traks Secures Contract to Manage Trackside Acoustic Detection System [Internet] [Accessed 2021 June 7] Available from: https://www.builtincolorado.com/blog/datatraks-secures-contract-manage-trackside-acoustic-detection-system-tads

[8] Ose, Mixanikos. "Heat Detectors-box and Brake Disc (Hot Box & Hot Wheel Detection System)." Heat Detectors-box and Brake Disc (Hot Box & Hot Wheel Detection System). N.p., 23 July 2021. Web.

[9] Tarawneh, C, Aranda, JA, Hernandez, VV, & Ramirez, CJ. "An Analysis of the Efficacy of Wayside Hot-Box Detector Data." Proceedings of the 2018 Joint Rail Conference. 2018 Joint Rail Conference. Pittsburgh, Pennsylvania, USA. April 18–20, 2018. V001T02A012. ASME. https://doi.org/10.1115/JRC2018-6218

[10] Cuanang, J, Tarawneh, C, Amaro, M, Jr., Lima, J, & Foltz, H. "Optimization of Railroad Bearing Health Monitoring System for Wireless Utilization." Proceedings of the 2020 Joint Rail Conference. 2020 Joint Rail Conference. St. Louis, Missouri, USA. April 20–22, 2020. V001T03A007. ASME. https://doi.org/10.1115/JRC2020-8060

[11] R. Estrada, Applications of Magnetostrictive Materials in the Real-Time Monitoring of Vehicle Suspension Components. Master of Science in Engineering (MSE), December 2014.

[12] J. N. Bensen, Energy Harvesting Techniques to Power Onboard Railway Bearing Condition Monitoring Systems. Master of Science in Engineering (MSE), August 2019.

[13] Mishra M., Mahajan P., Garg R. (2021) “Piezoelectric Energy Harvesting System Using Railway Tracks” Innovations in Electrical and Electronic Engineering. Lecture Notes in Electrical Engineering, vol 661. Springer, Singapore. https://doi.org/10.1007/978-981-15-4692-1_19

[14] M. Vasisht, G.A Vashista, J. Srinivasan, S. K. Ramasesha, Rail Coaches with Rooftop Solar Photovoltaic Systems: A Feasibility Study; Energy 118 (2017) 684-691.

[15] D. Ahn, K. Choi, Performance Evaluation of Thermoelectric Energy Harvesting System on Operating Rolling Stock, Micromachines 2018, 9, 359, doi:10.3990/mi9070359

[16] Batteries: Which one is the best? [Internet] [Accessed 2021 August 18] Available from: https://missionengineering.com/batteries-which-one-is-the-best/

[17] 1A Standalone Linear Li-Ion Battery Charger with Thermal Regulation in SOP-8 Datasheet [Internet] [Accessed 2021 July 3] Available from: http://www.tp4056.com/d/tp4056.p

[18] Open Railway Map [Internet] [Accessed 2021 July 3] Available from: https://www.openrailwaymap.org/index.php

[19] Calc Maps [Internet] [Accessed 2021 July 3] Available from: https://www.calcmaps.com/map-distance/

APPENDIX A

OTHER TESTING RESULTS

Table 29 Results for Route 2 at 100% railcar load using the four-second algorithm at a 0-minute interval – healthy bearing

Time [h]	Speed [rpm]/ [mph]	Avg. T_{amb} [°C]	Avg. T_{adp} [°C]	ΔT [°C]	Input Charge [mAh]	Output Charge [mAh]	Voltage [V]	Avg. Power Generated [mW]	Avg. Power Consumed [mW]
0.45	234/25	20	36	16	0.34	-0.17	3.84	1.3	-1.5
2.1	327/35	20	38	19	2.90	-1.37	3.85	11.2	-2.5
0.43	514/55	19	43	24	1.37	-0.34	3.95	5.3	-3.0
0.2	420/45	20	46	26	0.85	-0.17	3.96	3.3	-3.3
1.61	560/60	19	52	33	10.58	-1.05	3.98	41.0	-2.5
0.5	514/55	19	54	35	3.93	-0.17	3.98	15.3	-1.3
1	420/45	19	49	30	5.63	-1.87	3.99	21.9	-7.3
2.1	327/35	19	41	21	3.07	-1.37	3.98	11.9	-2.5
2.7	234/25	20	35	15	0.45	-1.54	3.98	1.7	-2.2
Total:					29.12	-8.05			

Table 30 Results for Route 2 at 100% railcar load using the four-second algorithm at a 0-minute interval – defective (cup spall) bearing

Time [h]	Speed [rpm]/ [mph]	Avg. T_{amb} [°C]	Avg. T_{adp} [°C]	ΔT [°C]	Input Charge [mAh]	Output Charge [mAh]	Voltage [V]	Avg. Power Generated [mW]	Avg. Power Consumed [mW]
0.45	234/25	20	34	14	0.68	-0.17	3.85	2.6	-0.7
2.1	327/35	20	37	17	4.44	-1.20	3.85	17.1	-4.6
0.43	514/55	19	41	22	1.71	-0.34	3.86	6.6	-1.3
0.2	420/45	20	43	23	1.02	-0.17	3.86	3.9	-0.7
1.61	560/60	19	50	31	13.48	-1.72	3.88	52.3	-6.7
0.5	514/55	19	51	33	4.51	-0.17	3.89	17.5	-0.7
1	420/45	19	47	28	6.93	-0.51	3.89	26.9	-2.0
2.1	327/35	19	40	20	5.46	-1.20	3.88	21.2	-4.7
2.7	234/25	20	34	14	1.20	-1.53	3.88	4.7	-5.9
Total:					39.43	-7.01			

Table 31 Results for Route 2 at 17% railcar load using the four-second algorithm at a 0-minute interval – healthy bearing

Time [h]	Speed [rpm]/ [mph]	Avg. T_{amb} [°C]	Avg. T_{adp} [°C]	ΔT [°C]	Input Charge [mAh]	Output Charge [mAh]	Voltage [V]	Avg. Power Generated [mW]	Avg. Power Consumed [mW]
2.7	234/25	19	26	7	0.00	-1.54	3.86	0.0	-6.0
2.1	327/35	19	27	8	0.00	-1.19	3.87	0.0	-4.6
1	420/45	19	29	10	0.00	-0.51	3.87	0.0	-2.0
0.5	514/55	19	31	12	0.00	-0.34	3.87	0.0	-1.3
1.61	560/60	18	34	16	0.00	-0.86	3.87	0.0	-3.3
0.2	420/45	18	37	19	0.00	-0.17	3.87	0.0	-0.7
0.43	514/55	18	36	18	0.17	-0.34	3.87	0.7	-1.3
2.1	327/35	19	33	14	0.34	-1.19	3.87	1.3	-4.6
0.45	234/25	19	30	10	0.17	-0.35	3.87	0.7	-1.4
Total:					0.68	-6.49			

Table 32 Results for Route 2 at 17% railcar load using the four-second algorithm at a 0-minute interval -defective (cup spalled) bearing

Time [h]	Speed [rpm]/ [mph]	Avg. T_{amb} [°C]	Avg. T_{adp} [°C]	ΔT [°C]	Input Charge [mAh]	Output Charge [mAh]	Voltage [V]	Avg. Power Generated [mW]	Avg. Power Consumed [mW]
2.7	234/25	19	24	5	0.00	-1.54	3.87	0.0	-6.0
2.1	327/35	19	25	6	0.00	-1.36	3.87	0.0	-5.3
1	420/45	19	27	8	0.00	-0.68	3.87	0.0	-2.6
0.5	514/55	19	28	9	0.00	-0.17	3.87	0.0	-0.7
1.61	560/60	18	30	12	0.00	-1.03	3.87	0.0	-4.0
0.2	420/45	18	32	14	0.00	-0.17	3.87	0.0	-0.7
0.43	514/55	18	31	13	0.00	-0.34	3.87	0.0	-1.3
2.1	327/35	19	29	11	0.00	-1.20	3.86	0.0	-4.6
0.45	234/25	19	27	8	0.00	-0.34	3.86	0.0	-1.3
Total:					0.00	-6.83			

APPENDIX B

MATLAB® CODE

```
clear all; close all; clc;
answer = newid('Experiment: ', 'Supply the following info.',1);
answer6 = questdlg('Is this for the SBT or 4BT?', 'Supply the following
info.','SBT','4BT','4BT');
answerstring = char(answer);
pad = 1;
differential = 1;
accel = 4;
switch answer6
case 'SBT'
locat = {'IB-SA' 'IB-M' 'OB-SA' 'OB-M' 'Prelim. Threshold' 'Maximum
Threshold'};
tester = 1;
case '4BT'
locat = {'B2-SA' 'B2-M' 'B3-SA' 'B3-M' 'Prelim. Threshold' 'Maximum
Threshold'};
tester = 0;
end
path = ['Z:\01 Experiments\' answer{1} '\ADXL\'];
da = dir(path);
ga = {da.name};
count = 0;
q = regexp(ga,'_');
index = cellfun(@(x) length(x)==2, q);
ga = ga(index);
if length(ga) >= 10
ga = [ga(10:length(ga)) ga(1:9)];
end
minthresh = [];
maxthresh = [];
BT0 = [];
BT1 = [];
BT2 = [];
BT3 = [];
BT4 = [];
BT5 = [];
BT6 = [];
BT7 = [];
T4 = [];
T5 = [];
T6 = [];
T7 = [];
T8 = [];
T9 = [];
T10 = [];
T11 = [];
AMB1 = [];
AMB2 = [];
MPwr = [];
H = [];jo = 0;
jo1 = 0;
jay = 0;
rpm3 = [];
```

```
date1=[];
time = [];
ctrl = [];
rpm4 = [];
pretime = [];
pretime2 = [];
newHavest=[];
progress = (1/length(ga));
Topbou = 100;
% Parameter set up
sbs = 4;
%seconds between samples
sampling = 5120;
%samples collected each iteration
SL = sampling*sbs;
%calculates the sample length
ix = cellfun(@(x) regexp(x,'_'),ga,'UniformOutput',0);
ax = cellfun(@(x) x(1),ix);
temp2 = [];
for qq = 1:length(ga)
temp = ga(qq);
temp2(qq,1) = str2num(temp{1}(1:ax(qq)-1));
end
temp3 = [temp2 [1:length(temp2)]'];
temp3 = sortrows(temp3);
ga = ga(temp3(:,2));
% Analysis
progressbar('Parsing through all speeds and loads...');
%Havest Protocol
for i = 1:length(ga)
    p = [path ga{i}];
    dd = dir([p '\Temperature*.lvm']);
    ddd = dir([p '\HarvestingVoltage*.lvm']);
    nn = length(dd);
    nnn = length(ddd);
    check = regexp(p, '_');
    for q = 1:nn
%loops through all of the files
    end
    if nn > 0
        for q = 1:nn
%loops through all of the files
          file = fullfile(p,dd(q).name);
%extracts file name
          rawtemp = dlmread(file,'\t',23,0);
%extracts data from file
          yy = length(rawtemp(:,1));
          pretime = floor(rawtemp(:,1))-floor(rawtemp(1,1));
            if jo == 0
              time(jo+1:jo+yy,1) = pretime(:,1);
            else
              if numel(pretime) == 1
                 time(jo+1:jo+yy,1) = 2*time(jo,1) - time(jo-1,1);
              else
                  pretime2(:,1) = pretime(:,1) + pretime(2,1);
                  time(jo+1:jo+yy,1) = time(jo,1)+ + pretime2(:,1);
              end
```

```
           end
         if tester == 1
             %Bayonet Thermocouples
             BT0(jo+1:jo+yy,1) = rawtemp(:,2);
             BT1(jo+1:jo+yy,1) = rawtemp(:,3);
             BT2(jo+1:jo+yy,1) = rawtemp(:,4);
             BT3(jo+1:jo+yy,1) = rawtemp(:,5);
             %Regular Thermocouples
             T4(jo+1:jo+yy,1)  = rawtemp(:,6);
             T5(jo+1:jo+yy,1)  = rawtemp(:,7);
             T6(jo+1:jo+yy,1)  = rawtemp(:,8);
             T7(jo+1:jo+yy,1)  = rawtemp(:,9);
             T8(jo+1:jo+yy,1)  = rawtemp(:,10);
             T9(jo+1:jo+yy,1)  = rawtemp(:,11);
             T10(jo+1:jo+yy,1) = rawtemp(:,12);
             T11(jo+1:jo+yy,1) = rawtemp(:,13);
            % Ambient Temperatures
             AMB1(jo+1:jo+yy,1) = rawtemp(:,15);
             AMB2(jo+1:jo+yy,1) = rawtemp(:,14);
         else
             % Bayonet Thermocouples
             BT0(jo+1:jo+yy,1)   = rawtemp(:,2);
             BT1(jo+1:jo+yy,1)   = rawtemp(:,3);
             BT2(jo+1:jo+yy,1)   = rawtemp(:,4);
             BT3(jo+1:jo+yy,1)   = rawtemp(:,5);
             BT4(jo+1:jo+yy,1)   = rawtemp(:,6);
             BT5(jo+1:jo+yy,1)   = rawtemp(:,7);
             BT6(jo+1:jo+yy,1)   = rawtemp(:,8);
             BT7(jo+1:jo+yy,1)   = rawtemp(:,9);
             % Regular Thermocouples
             T1(jo+1:jo+yy,1)  = rawtemp(:,10);
             T2(jo+1:jo+yy,1)  = rawtemp(:,11);
             T3(jo+1:jo+yy,1)  = rawtemp(:,12);
             T4(jo+1:jo+yy,1)  = rawtemp(:,13);
             % Ambient Temperatures
             AMB1(jo+1:jo+yy,1)  = rawtemp(:,14);
             AMB2(jo+1:jo+yy,1)  = rawtemp(:,15);
             % Adapter Temperatures
             ADAP1(jo+1:jo+yy,1) = rawtemp(:,16);
             ADAP2(jo+1:jo+yy,1) = rawtemp(:,17);
         end
         jo = jo+yy;
         rawtemp = [];
         yy = [];
         pretime = [];
         pretime2 = [];
        end
      if nnn > 0
          for w = 1:nnn
%loops through all of the files
          file = fullfile(p,ddd(w).name);
%extracts file name
          Havest = dlmread(file,'\t',23,1);
%extracts data from file
          hh = length(Havest(:,1));
          pretime = floor(Havest(:,1))-floor(Havest(1,1));
           if jo1 == 0
```

```
            timeq(jo1+1:jo1+hh,1) = pretime(:,1);
     else
         if numel(pretime) == 1
             timeq(jo1+1:jo1+hh,1) = 2*timeq(jo1,1) - timeq(jo1-1,1);
             else
             pretime(:,1) = pretime(:,1) + pretime(2,1);
             timeq(jo1+1:jo1+hh,1) = timeq(jo1,1)+ + pretime(:,1);
         end
     end
   if tester==1
       H(jo1+1:jo1+hh,1) = Havest(:,1);
   else
       H(jo1+1:jo1+hh,1) = Havest(:,1);
   end
   jo1 = jo1+hh;
   Havest = [];
   hh = [];
     end
      end
    end
    progressbar(progress*i);
    if tester == 1
        Bavg = mean([BT0 BT1 BT2 BT3]');
        Tavg = mean([T4 T5 T6 T7 T8 T9 T10 T11]');
    else
        Bearing = [(BT0+BT1)./2 (BT2+BT3)./2 (BT4+BT5)./2 (BT6+BT7)./2];
    end
    AMB = (AMB1'+AMB2')/2;
    Timeh = time/3600;

end
if tester ==1
figure(1)
plot(Timeh,H)
xlabel('Time [h]')
ylabel('Voltage [V]')
figure(2)
hold on;
plot(Timeh,T11,'r')
plot(Timeh,AMB1,'b')
xlabel('Time [h]')
ylabel('Temperature [\circC]')
legend('Adapter','Ambient')
else
figure(1)
plot(Timeh,H,'b')
xlabel('Time [h]')
ylabel('Voltage [V]')
figure(2)
hold on;
plot(Timeh,ADAP1,'r')
plot(Timeh,AMB1,'b')
xlabel('Time [h]')
ylabel('Temperature [\circC]')
legend('Adapter','Ambient')
end
```

BIOGRAPHICAL SKETCH

Martin Amaro Jr. was born in Edinburg, Texas on April 1st, 1996. He attended Edinburg North High School graduating in Spring of 2014. Martin then attended the University of Texas Rio Grande Valley where he received his bachelor's degree in mechanical engineering in May of 2019. Martin continued his education at the University of Texas Rio Grande Valley where he obtained his Master of Science in Mechanical Engineering degree in December of 2021. While Martin attended graduate school, he worked at the University Transportation Center for Railway Safety (UTCRS) where he helped his colleagues conduct research in railroad related applications. This will eventually lead for his own research to be published in journal and conference papers. This opportunity allowed Martin to later participate in the Dwight D. Eisenhower Transportation Fellowship Program. Martin Amaro Jr. can be reached at martin.amaro01@outlook.com